Product Development of Fully Recyclable Single-Use Coffee Cups

By

Pip Catchpole, MChem, BSc

September 2019

A thesis submitted for the degree of Masters by Research in Chemistry at Lancaster University, United Kingdom.

ACKNOWLEDGMENTS

ABSTRACT

Disposable cups are typically made from PE-lined paper. They are recyclable at specialist sites where their components are separated, however the cups must be isolated from all other waste prior to collection by recycling companies. PE is obtained from fossil fuels, although it can be acquired from crops such as sugarcane. To derive PE solely from crops, a lot of land would be needed to grow them, which is unrealistic. Regardless of the source, PE is non-biodegradable. This project aimed to develop a polymer that is from a renewable source, biodegradable, and/or easier to recycle. PLA and PHB were investigated as copolymers of varying compositions for their suitability to line cups. The 8 copolymers made all had melting points and thermal degradation temperatures significantly higher than the boiling point of water. All the copolymers were all melted onto uncoated cup paper and some tests were performed to assess their water permeability. The polymers with a higher percentage of BL in their composition (75% or higher) demonstrated better water resistance, when exposed to room temperature DI. Further testing is required using hot water.

ABBREVIATIONS

Abbreviation	Definition
%BL	Percentage composition of BL in the polymer
%LA	Percentage composition of LA in the polymer
BL	β-Butyrolactone
BP	Bis(phenolate)
CEM	Chain-end Stereocontrol Mechanism
CL	ε-caprolactone
Cumyl	2-Phenylpropane
DFT	Density Functional Theory calculations
DI	Deionised Water
DSC	Differential Scanning Calorimetry
DTG	Differential Thermogravimetry
EDX	Energy Dispersive X-ray Spectrometry
GPC	Gel Permeation Chromatography
HW2	Test where a polymer film sample was submerged in 95 °C DI water.
LA	Lactide
LDPE	Low Density Polyethylene
M_n	Number Average Molecular Weight
$M_{n, theo}$	Theoretical Number Average Molecular Weight
NMR	Nuclear Magnetic Resonance Spectroscopy
NOESY	Nuclear Overhauser Effect Spectroscopy
PCRRG	Paper Cup Recovery & Recycling Group
PDI	Polydispersity Index
PE	Polyethylene
PHB	Polyhydroxybutyrate
PLA	Polylactic acid
P_r	Probability of a racemic linkage
PTFE	Polytetrafluoroethylene
PXRD	Powder X-ray Diffraction
Rac	Racemic
RMM	Relative Molecular Mass
ROP	Ring-opening Polymerisation
SEM	Scanning Electron Microscope/Microscopy
T_o	Thermal Degradation Onset Temperature
T_c	Crystallisation Temperature
T_g	Glass Transition Temperature
TGA	Thermogravimetric Analysis
THF	Tetrahydrofuran
T_m	Melting Temperature
T_{max}	Temperature of Maximum Mass Loss
W2	Test where a polymer film sample was submerged in room temperature DI water.
w_c	Degree of Crystallinity
wt%	Weight percent

CONTENTS

1   LITERATURE REVIEW

1.1   INTRODUCTION

1.1.1 The Coffee Cup Problem

In 2011, it was estimated that 2.5 billion coffee cups are produced annually.[1] Of these, less than 1% are currently recycled.[2] The rest of the cups go to landfill. However, by the end of 2019, the Paper Cup Recovery & Recycling Group (PCRRG) speculate that 1 in 12 cups will be recycled.[3] Single-use beverage cups that are heatproof and leak-proof are made by lining paper with plastic.[4] This combination of materials is what makes the cups difficult to recycle, as they require a more complicated process than paper recycling.[2] This leads to cups being part of the many plastics that are problematic at the end of their life. They are part of an overwhelming majority of plastics that are discarded, or sometimes incinerated (**Figure 1**). If non-biodegradable plastics are discarded, they persist in the environment and accumulate.[5]
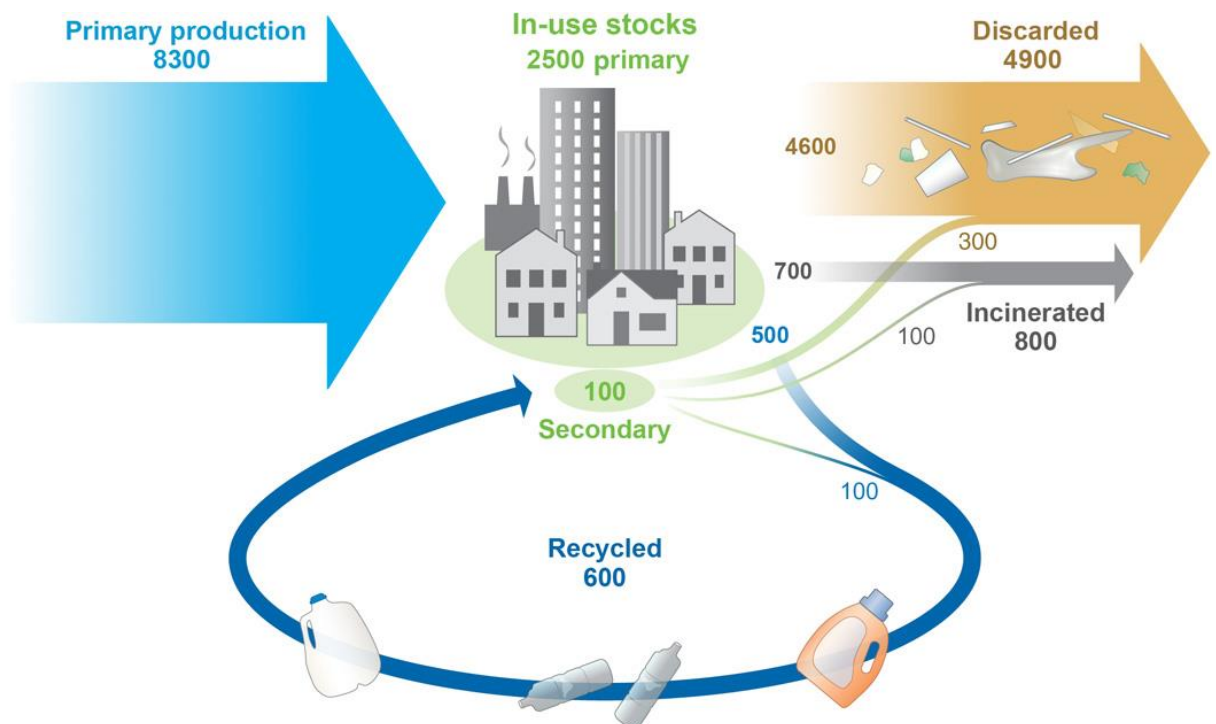
Figure 1: "Global production, use and fate of polymers and their derivatives (1950-2015; in million metric tons)." Figure reproduced with permission from ref.6

Product Development of Fully Recyclable Single-Use Coffee Cups

Some coffee shop chains have realised the environmental impact of their disposable cups so have become committed to recovering and recycling them. Costa aims to recycle the same number of cups as they put into the market annually by 2020.[7] Conversely, in June 2018, another coffee shop company (Boston Tea Party) banned single-use cups from their coffee shops. Customers must either drink inside the establishment, bring a re-useable cup, or pay a deposit on a reusable cup from the chain, which can be returned to any of their 21 branches. Despite the decrease in sales, the chain's owner (Sam Roberts) believes saving the planet is more important than his profits and is encouraging others to follow suit.[8] Pret A Manger and Starbucks both offer discounts on drinks if customers bring their own cups with Pret A Manger claiming they have saved 6 million paper cups from landfill. Caffè Nero, Starbucks, Greggs, McDonald's UK, and Pret A Manger are all involved in a cup recycling scheme to fund their single-use cups being collected for recycling.[8]

However, coffee cups are usually lined with polyethylene (PE) so even when they are recycled, there are limitations to how environmentally benign they can be (see section 1.1.2). In addition, the cups must be isolated from all other items, so they can be collected separately and transported to specialist recycling centres. This is not ideal as infrastructure would need to be put in place to collect coffee cups as an isolated item for recycling. This has an associated carbon footprint with the transportation.[4] Also, this system relies on consumers putting the disposable cups in the correct bin so they can be recycled, not sent to landfill or littered in the environment. However, there have been advancements in this area with Costa paying a £70 supplement per tonne of cups collected and recycled through 3 of the UK's cup recycling companies (DS Smith, James Cropper, and ACE UK). In October 2018, the PCRRG stated that this has made a tonne of cups worth an average £120 post-disposal, up from £50 in 2017.[9] In 2017, the Environmental Audit Committee recommended to the UK government that all single-use coffee cups that are disposed of in recycling bins should be recycled

by 2023. If this is not met, their recommendation was for the UK government to ban all disposable coffee cups. The Environmental Audit Committee believed that the waste issue of disposable coffee cups was, and is, an avoidable problem.[2]

In 2016, PCRRG launched its manifesto about increasing the recycling rates of single-use beverage cups. PCRRG is a group of companies and organisations from all levels of the cup supply chain, from paper manufacturers to coffee shops that are committed to improving the recovery and recycling of disposable cups. The PCRRG support the idea of a circular economy where the paper and plastic from the cups are both recycled.[9]

VTT Technical Research Centre of Finland Ltd. carried out a life cycle assessment on paper cups in 2018-2019. They found that ceramic cups had to be washed a minimum of 350 times before they had a smaller carbon footprint than that of paper cups. Similarly, steel reusable cups had to be washed at least 130 times to contribute less carbon emissions than a paper cup. Also, plastic reusable cups had to be reused at least 20 times before it had a smaller carbon footprint than a paper cup. If the single-use paper cup was recycled, the plastic reusable cup had to be reused at least 32 times for it to have a smaller carbon footprint.[10] However, this is an achievable target for a plastic reusable cup. In addition, it is likely that a ceramic cup could be used 350 times or more in a coffee shop setting.

Single-use coffee cups are mostly made from wood fibre, which can be sustainably harvested. These forests and their paper products store carbon. With a demand for paper product, comes a need for sustainable forests, which helps combat atmospheric CO_2.[11] This, combined with the life cycle assessment discussed in the previous paragraph, means creating a more environmentally friendly single-use coffee cup is a viable endeavour.

One of the companies interested in a more environmentally benign single-use beverage cup are the Printed Cup Company, based in Clitheroe, Lancashire. They make bespoke single-use beverage cups, therefore have sponsored this project and provided an industry insight into the problem.

1.1.2 PE Lining

Ethylene monomers are typically sourced from fossil hydrocarbons and polymerised into PE, which is a non-biodegradable thermoplastic. PE can also be sourced from bioethanol that is derived from sugarcane.[12] Although, the PE is still non-biodegradable. It accumulates in landfills and the only way to degrade it is by combustion methods.[6] The low density PE (LDPE) that is used for lining single-use beverage cups is not a plastic that is typically recycled as part of household collections.[13] LDPE is also used to make plastic bags and six-pack rings (used for holding 6 drinking cans together), which are often described as the plastic products causing the most pollution.[14] In 2017, Coda reported that only 5% of LDPE that is produced gets recycled due to difficulties in separating this plastic from others and difficulties in recycling.[14] However, when the disposable coffee cups are isolated from other waste and collected, both the paper and the plastic lining can be recycled.[9]

LDPE is ideal for use as a lining for coffee cups, as its melting temperature (T_m) is 111-112 ° C, higher than the temperature of boiling water. This leads to good thermal resistance. PE also possesses good chemical resistance, flexibility, and ease of processing through thermoplastic methods such as extrusion.[15] The glass transition temperature (T_g) is defined as the temperature at which the polymer changes from a glassy state to a polymer melt. During this transition, the heat capacity of the sample changes, without the volume or enthalpy changing.[16] For LDPE, the T_g occurs at -125 °C,[17] hence its flexibility at room temperature. When processed into a film, its surface is inert, non-porous, and hydrophobic.[15] This makes LDPE ideal for lining a coffee

cup as it will not react with the cup contents and it will not allow the contents to be exposed to the paper.

There are a few specialist companies in the UK that can recycle the coffee cups currently in circulation. One of them is James Cropper, which launched a programme called Cup Cycling™ in September 2017. They recycle single-use beverage cups by recovering the paper pulp to make paper products, such as packaging. Since launching, they have recycled over 30 million coffee cups into paper-based packaging, with the capacity to recycle 500 million cups per year.[18] They send the plastic to other companies to be recycled into other plastic items.[9]

1.1.3 Coffee Cup Requirements

Coffee cups need to be able to withstand being exposed to boiling water. In addition, coffee is acidic, having a pH between 4.90-6.18 as found by Moon *et al.* (depending on the origin of the coffee bean and its subsequent treatment).[19] Therefore, the cups need to remain heatproof and leak-proof under acidic conditions at 100 °C. Moreover, the polymer needs to be a thermal insulator to some extent to keep the drink warm for a reasonable amount of time. As well as this, the lining needs to be biocompatible so that it is safe to be in contact with the beverage. It needs to be classed as food-safe and to be non-permeable. Furthermore, the polymer should not affect the flavour of the coffee itself, and not produce an odour even when hot drinks are added to the cups. To improve on the PE lining, the polymer needs to be from a renewable source and be biodegradable and/or more easily recyclable.

In addition, melting of the polymer is what forms the seam down the side of the cups and keeps the bottom insert of the cup in place. The new polymer also needs to melt and form watertight seams when made into a cup. This is an important feature so that the current manufacturing process can still be used, saving cup manufacturers money as they will not need new cup forming equipment. Also, it is important that more materials are not required to make the cups (e.g. a glue to form the seam) which would add to the cost of manufacture.

1.2 POLYMER SELECTION

Given the issues discussed in section 1.1 relating to the current PE lining in coffee cups, a solution is needed to create a more environmentally benign single-use beverage cup. A possible solution is to replace the PE with a more eco-friendly polymer; therefore, it is important to examine the properties of other polymers.

Aliphatic polyesters are a class of polymers commonly looked at when searching for environmentally friendly plastic alternatives. They have good mechanical properties and are biocompatible. They can be bio-based (i.e. derived from a renewable source) and biodegradable (meaning they degrade into simple molecules, such as carbon dioxide and water, under environmental conditions).[5] They can be synthesised via ring opening polymerisation (ROP) processes, which tend to have close to 100% atom economy. Additionally, there are numerous cyclic esters available from renewable sources that can be used as monomers. ROP of cyclic esters has become a desirable process for green chemistry.[20]

1.2.1 PLA

Polylactic acid (PLA) is formed by polymerising lactide (LA), which is derived from starch-rich products such as corn, sugar beet, tapioca and wheat.[20] Starch is stored in the non-photosynthetic parts of the plants such as seeds, roots and stems. These starch stores are extracted for industrial use.[21] Plants synthesise starch as a result of photosynthesis.[22] This starch is converted to sugar, which is fermented to produce lactic acid (**Figure 2**). Water is removed to form LA.[23] Polymerisation affords PLA for use in products. At the end of its use, PLA can be degraded, which converts it into carbon dioxide and water.[24]
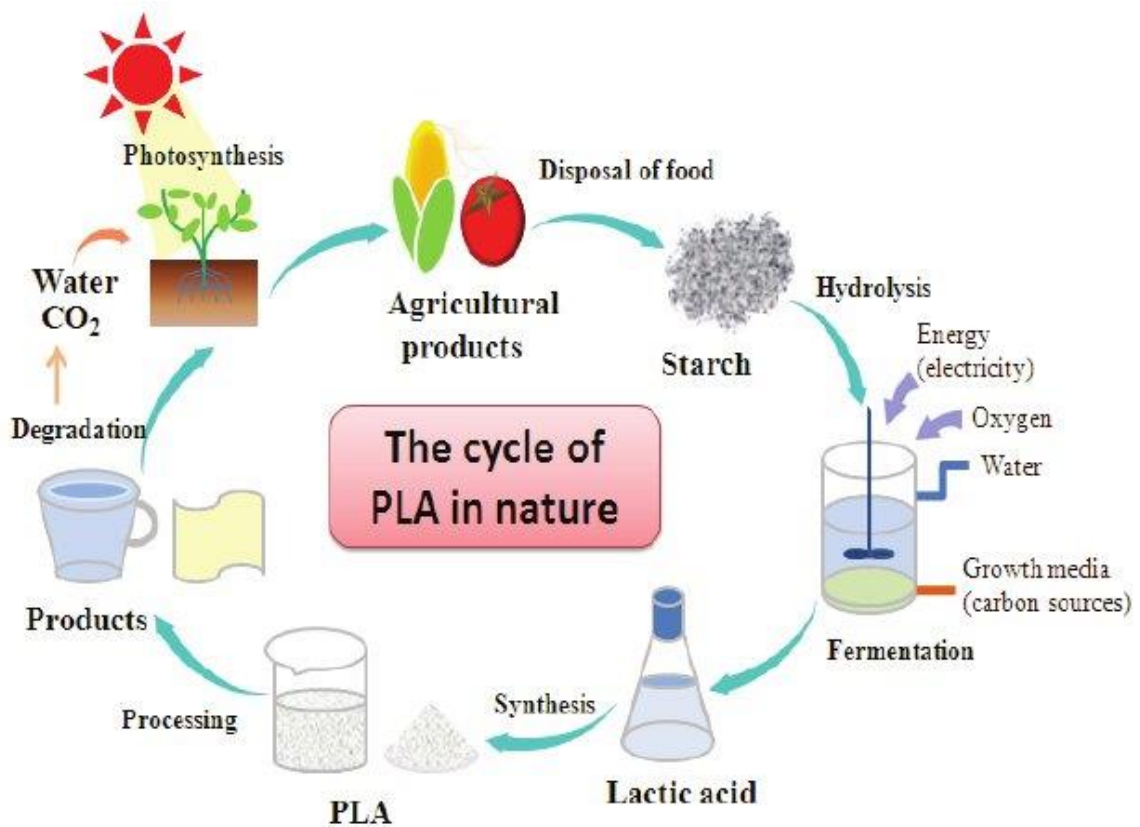
Figure 2: The cycle of PLA in nature before and after use as a commercial product. Figure and caption reproduced with permission from ref.22

LA exists as two enantiomers that create two optically active configurations: L-LA and D-LA (**Figure 3**). Racemic (*rac*) LA is a 50:50 mixture of the L-LA and D-LA. The ratio of L/D enantiomers in the blend affects the macromolecular properties of the PLA such as T_m and degree of crystallinity (w_c).[25] W_c is the mass or volume fraction of the crystalline phase of a polymer sample, where the crystalline phase refers to the parts of the sample that have 3 dimensional, long-range atomic order.[16] Poly(*D*-lactic acid) and Poly(*L*-lactic acid) both have regular chain structures and are crystalline materials. Mixing the two decreases the w_c.[26] Polymerising *rac*-LA affords poly(*D,L*-lactic acid) which is an amorphous polymer.[22] Amorphous refers to a sample or phase (part of a sample) lacking long-range atomic order.[16]

<div align="center">

D-lactide | L-lactide | meso-lactide
R, R - lactide | S, S - lactide | S, R - lactide

</div>
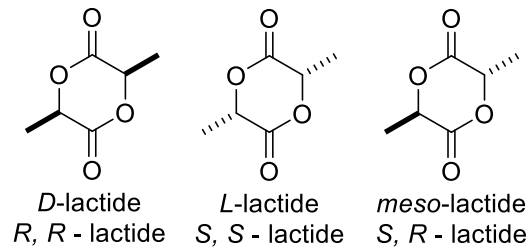
Figure 3: The three possible enantiomers of LA. *Rac*-LA is a mixture of the D and L enantiomers.

PLA has high mechanical strength, good thermoforming ability[20] (i.e. can be heated into a pliable form so that it can moulded into the desired shape[27]), biocompatible, and is from a renewable source. It can be processed through the current plastic processing methods due to its similarities with petroleum-based plastics. However, it produces 15-60% less carbon emissions and lowers the energy consumption required for moulding by 25-55%.[20] It also has lower environmental impact compared to petroleum-based plastics with respect to fossil fuel resources and recycling opportunities.[20] 20-50% Less fossil fuel resources are required to produce PLA than the equivalent petroleum based polymers.[24]

PLA has a T_m of 160-170 °C[24] and a T_g of 60-70 °C.[28] It is important to note that low molecular weight PLA has a lower thermal degradation temperature due to a self-catalytic degradation mechanism.[29] Also, whilst PLA is biodegradable, it degrades slowly[20] due to the slow hydrolysis of the ester backbone, meaning PLA can take several years to degrade.[22] In addition, LA is sourced from biomass; forests would need to be cleared to grow starch-rich crops to replace all the current petroleum-based plastics with just PLA. Associated with this, excessive water and pesticide use would be required which has environmental and health impacts.[25] Also, this land could be used to grow crops for food in countries that are struggling to feed their population, instead of for plastics in first world countries.

The current proposed methods for processing PLA at the end of its life are landfilling, incineration, and composting.[30] In landfill, no energy is

recovered from the PLA and it degrades very slowly. When incinerated, feedstock energy can be recovered and carbon dioxide is emitted into the atmosphere.[31] PLA can be degraded by hydrolysis into oligomers, a process which is both temperature and humidity dependent. High humidity and 55-70 °C temperature are required,[32] which is very specific and does not mean PLA is easy to compost. Microorganisms typically present in soil can then break the oligomers down into carbon dioxide and water.[32] In addition, there is the potential to recycle PLA. Lopez *et al.*[33] found that PLLA (PLA made from solely L-LA) can be recycled up to 5 times without a significant change to its properties after mechanical recycling (the plastic is shredded into pellets and used as raw material).[33] However, it is difficult to separate from other plastics as it is indistinguishable from polyethylene terephthalate.[34] Therefore, it is currently difficult to recycle PLA due to isolation issues.

PLA is also already approved for use in food packaging due to its biocompatibility.[20] It is currently used for various products including bottles, trays, and films for food packaging.[35] However, its use is somewhat limited due to its low impact resistance, and poor crystallisation performance.[35] Increasing the w_c of PLA increases its barrier performance[36] (the "materials' ability to prevent the transmission of moisture or oxygen"[37]). This can be done by incorporating polyhydroxybutyrate (PHB).[36] PLA is also prone to thermal degradation during processing whilst it is in a molten state. This degradation is dependent on the purity of the PLA, the processing temperature and how long it is exposed to the higher temperatures.[38] This can also cause issues during recycling of PLA, although blending it with another polymer can improve its properties.[35]

1.2.2 PHB

PHB is biodegradable and biocompatible.[39] It is produced as a storage material in some bacteria[40] when they are lacking a non-carbon based nutrient (such as nitrogen), and have plentiful amounts of carbon from sources like carbohydrates.[36] It is produced via a series of reactions

involving enzymes, where only the *R*-configuration of the polymer is produced.[41] The bacteria also degrade PHB when they are no longer deprived of nutrients (**Figure 4**).[42] Commercially, PHB is made by bacteria through fermentation of carbohydrates.[43] PHB is one of the more expensive bioplastics due to the costs associated with bacterial fermentation.[40] Currently, there are investigations into development of transgenic organisms that produce PHB in a faster, cheaper way.[42] However, this would lead to similar issues as discussed with growing crops to produce PLA (see section 1.2.1).
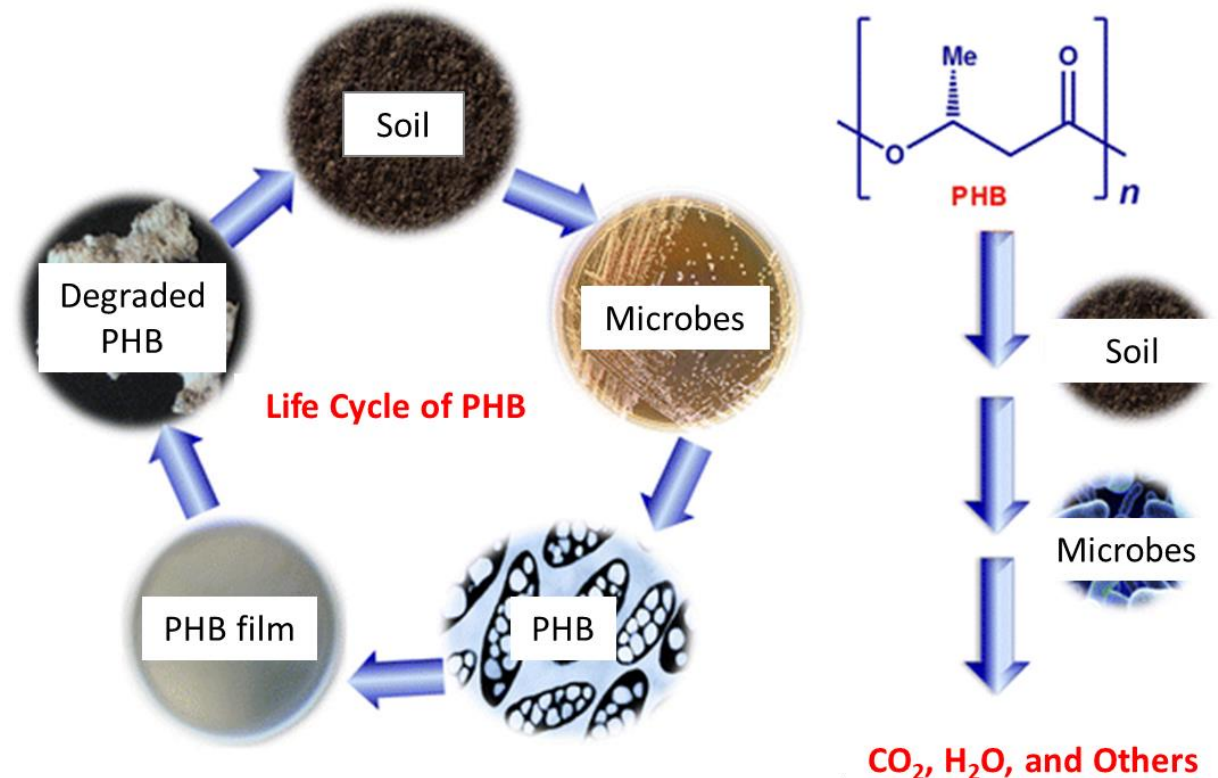
Figure 4: Life cycle of PHB. Figure adapted from ref.44

The asymmetric centre present in β-butyrolactone (BL) allows two possible enantiomers to be formed (**Figure 5**) and this chirality is transferred to the polymer. The *R*-configuration of the polymer is preferable as the stereochemistry affects the biocompatibility and biodegradability.[41]

S-*β*-Butyrolactone   R-*β*-Butyrolactone
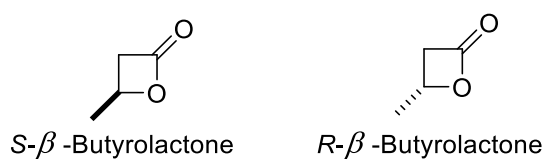
Figure 5: Two enantiomers of BL.

PHB can also be chemically recycled by thermal degradation into crotonic acid, a cyclic trimer, and linear oligomers with a crotonate end group (**Figure 6**).[45]
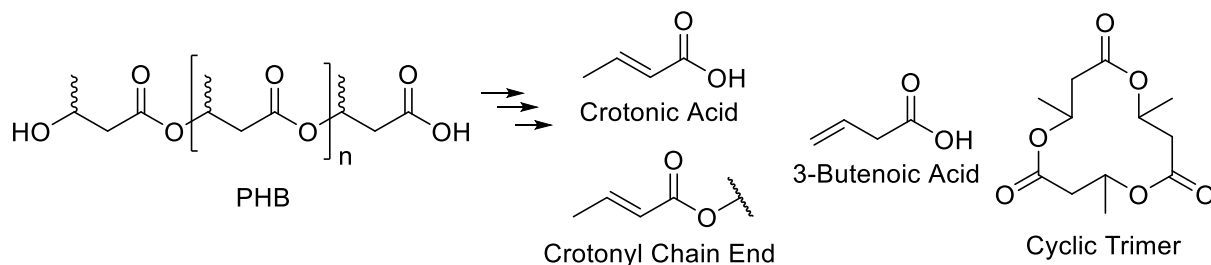
Figure 6: Potential products from thermal degradation of PHB. Figure adapted from ref.45

Isotactic PHB is a renewable thermoplastic.[40] When all the asymmetric centres are of the *R*-configuration and the polymer is of high molecular weight, linear, and highly crystalline. It has physical and mechanical properties that are similar to some of the petroleum-based polymers, such as polyethylene terephthalate.[43]

However, PHB has some shortcomings. Its mechanical properties are poor, due to its high w_c, making PHB brittle. This has limited its potential applications.[46] Its melting point is 165-180 °C[45,47], which is considerably lower than its thermal degradation temperature at around 285 °C.[43,47] The processing temperature of PHB should be a minimum of 180-190 °C. The thermal degradation of PHB begins at these temperatures with chain scission that results in a decrease in molecular weight.[46] Lai *et al.* found that heating PHB to 190 °C for various lengths of time resulted in BL oligomers being formed. They determined the number average molecular weight (M_n) and polydispersity index (PDI) of the PHB samples before heating and at various times throughout the heating process which lasted up to 120 minutes. They reported a decrease in M_n from 110.2×10^3 g/mol to 43.9×10^3 g/mol after just 10 minutes at 190 °C. After 20 minutes, it dropped to 7.4 kg/mol and by the end, at 120 minutes; the M_n was just 1.6×10^3 g/mol. The PDI remained reasonably constant throughout and ranged between 1.25-1.61. However, as the M_n dropped, so did the T_g from 2.4 °C before

heating, to -13.6 °C after 120 minutes at 190 °C.[48] This thermal instability can lead to problems during melt processing.[45]

Bacterial fermentation is a costly process to synthesise PHB, however an alternative synthetic route is possible via ROP of commercially available BL. This is more cost effective and allows control over stereochemistry, tacticity, end groups, and molecular weight. By producing syndiotactic enriched PHB, it is possible to modulate the thermal properties.[43] The molecular weight and tacticity of PHB does not affect the thermal degradation temperature.[49]

Altaee *et al.*[44] measured the biodegradation rate of PHB films by measuring the mass of the films before burying them in soil, then measuring the mass again after 6 weeks. The soil used had a pH of 7.3 and was in a fertile garden. The humidity was 80% at 30 °C. Film samples were placed in non-degradable meshed bags and buried 10 cm below the surface of the soil. For PHB, the M_n dropped by 26%, with the PDI remaining similar at 1.72 and 1.54 before and after the experiment. The mass of the PHB films decreased by 62% over the 6 weeks. They also found that the number of microorganisms present in the soil increased over time. In summary, Altaee *et al.* found that PHB can be degraded by microorganisms present in fertile soil to cause a significant mass decrease in as little as 6 weeks.[44] This demonstrates that PHB can biodegrade rapidly under the correct conditions.

1.2.3 PLA-PHB Blend

On an industrial scale, melt blending two polymers is simple, cost effective, and the equipment needed is already easily available.[36] The miscibility of two polymers in a blend affect the T_g, T_m, w_c, and the morphology of the polymer matrix. These properties have a direct effect on the macroscopic properties of the material such as ease of processing, barrier properties with respect to water and oxygen, and degradation behaviour.[50] For example, PHB is brittle on its own, but blending it with another polymer can alter this. Also, the

biodegradability of PHB can be improved by blending it with another polymer.[33]

Zhang *et al.*[51] carried out a study on PHB/PLA blends. They made the blends by dissolving a combined total of 3% weight per volume of the polymers in chloroform. The films were made by solvent casting which involved evaporating the solvent at room temperature and then vacuum drying the films for 24 hours. Differential scanning calorimetry (DSC) was then used to analyse the varying thermal properties and w_c values of the various polymer blends. It was found that the w_c decreased with increasing amounts of PLA content. However, the T_m remained constant and there were consistently two distinct T_g values corresponding to the PHB and PLA components. This data suggested immiscibility of the blends. They also compared the solvent casting method for blending the polymers with melt blending. They did this by magnetically stirring the blend solution and evaporating the solvent under reduced pressure. The residue was heated at 190 °C for 30 minutes. They found the DSC thermogram of the equivalent solvent casted and melt blended polymers to have different looking peaks. The melt blended T_m peaks were broader and the T_g values were lower than the equivalent solvent-casted blends. Zhang *et al.*[51] suggested that this shows greater miscibility of the polymers when they are melt blended. They theorised that these results could be due to transesterification occurring between the PHB and PLA chains, when they are heated to 190 °C for 30 minutes, to produce block copolymers. They concluded that amorphous PHB and PLA were immiscible, and that heat treatment increased the miscibility (possibly due to transesterification). The w_c of PHB was decreased by addition of amorphous PLA. The change in crystallisation caused a decrease in T_m and w_c after heat treatment. Also, hydrolytic degradation rate of PHB is increased by addition of PLA.[51] Based on this work, co-polymerisation could lead to greater polymer agreeability as the melt blended polymers had greater miscibility, possibly due to transesterification reactions. In addition, the hydrolytic degradation of PHB was increased by addition

of PLA. This has potential to increase the biodegradability rate of PHB in water.

Arrieta *et al.*[49] used thermogravimetric analysis (TGA) to determine the performance of PHB and PLA. They made polymer blends by mixing 75:25 ratio of PLA:PHB and heating to 180 °C with stirring for 4 minutes. Films were made by compressing the blend at 180 °C in a hot press. The average film thickness was 200 μm ± 50 μm. Both the pure polymers and the PLA/PHB blend were heated up to 450 °C. Both the homopolymers showed a steep mass loss at their thermal degradation onset temperatures (T_o) of 261 °C and 315 °C for PHB and PLA respectively. The blended polymer degraded in two steps with T_o of the first step being interpreted as the degradation of PHB and the second as the degradation of PLA. The T_m of PLA was found to be 167.3 °C; PHB was 174.2 °C with the blend being similar to PLA at 167.4 °C. The w_c of the three polymers was 5.1% for PLA, 40.7% for PHB, and 16.4% for the PLA/PHB blend. This suggested that the crystallinity of PLA can be increased by blending it with PHB.[49] Increased crystallinity is desirable as the film forms a better barrier with respect to oxygen and water vapour. This is because the more crystalline the material, the more indirect the path for the molecules to travel through the film by reducing the mobility of the polymer chains.[52]

Arrieta *et al.*[49] also investigated the water contact angle of the polymers. This is an indirect way of measuring the surface wettability. This is interesting for polymers that are destined for food packaging applications as the surface wettability has a direct effect on the properties of the films. Such properties affected include: water vapour permeability, adhesion, printing, and commencement of biodegradation.[36] The water contact angle of PLA was found to be 58.4 °, for PHB it was 61.3 °, and for the 75:25 PLA:PHB blend it was 70.0 °. The more hydrophobic a surface is, the higher the water contact angle is, with an angle over 65 ° classifying a surface as hydrophobic, and those lower as hydrophilic. By this reasoning, PLA and PHB are classed

as hydrophilic but their blend is hydrophobic. They concluded that the crystallinity of PLA was increased by blending with PHB. Also, that the extent of water incorporation was lowest in the blend compared to the pure polymers.[49] In contrast to Arrieta *et al.*, a study by Puglia *et al.*[53] determined the water contact angle of PHB to be 76 ° and therefore hydrophobic.[53] In addition, a study by Jorda-Vilaplana *et al.*[54] determined the water contact angle of PLA to be 73.4 ° and therefore hydrophobic.[54] These results are significantly different. These reported contact angles are all considerably lower than the water contact angle of LDPE which was reported by Fombuena *et al.* to be 100.05 °.[15] Thus, PLA and PHB have higher wettability than LDPE. However, as a copolymer, they could be hydrophobic enough to use in a disposable cup.

Lai *et al.*[48] also prepared PLA/PHB blends by melt blending. They heated a combination of the polymers in different ratios at 180 °C with stirring for 20 minutes. The blends were formed into pellets and hot pressed into a film at 180 °C. The blends were analysed using TGA from room temperature up to 500 °C. These blends showed a two-step degradation process with the first step being attributed to the PHB component and the second step being the PLA component. The temperature of maximum mass loss (T_{max}) of PHB was higher in the blends than the pure polymer. They theorised that this was due to the PLA having a shielding effect on the PHB. They also reported that the T_{max} of PLA was slightly lower when blended with PHB than as a pure polymer.[48] Therefore, PLA can increase the thermal resistance to degradation of PHB.

1.2.4 PLA-PHB Copolymer

Copolymers are polymers that have been made from more than one monomer. This is typically done to improve the properties of the product. Four types of copolymerisation are: random, block, graft, and alternating (**Figure 7**).[55]

a) Random

b) Block

c) Alternating

d) Graft

Figure 7: Four types of copolymer; yellow blocks represent a monomer and blue blocks represent a different monomer. Figure adapted from ref.55

Copolymerisation affords polymers with unique properties. It allows further control of the properties by varying the composition and monomer sequences as well as the molecular weight and other properties that can be altered in homopolymers. It can allow mechanical properties, thermal properties and degradation rates of the polymers to be fine-tuned for the desired purpose.[43]

Copolymerising PLA with another polymer can improve its properties without affecting its biodegradability.[20] As PLA offers good thermal and mechanical properties, as well as a higher degradation temperature, it could improve the properties of PHB by copolymerisation.[43]

Copolymerisation of LA and BL (**Figure 8**) is uncommon in the literature and seldom done with yttrium based catalysts,[43,56] despite yttrium catalysts efficiently producing syndiotactic enriched, high molecular weight PHB.[43] ROP of LA and BL has been reported with the use of stannoxane catalysts,[57] group 4 metals with amine tris(phenolate) ligands,[58] and aluminium with salan and salen type ligands.[59,60]
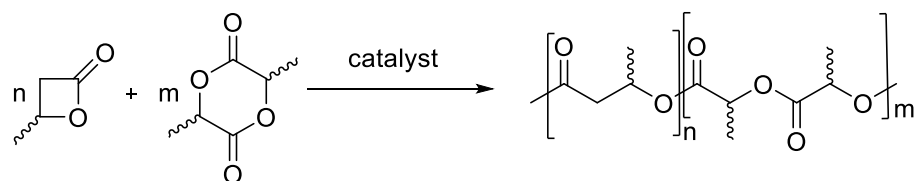
Figure 8: General reaction scheme for catalysed ROP of *rac*-BL and *rac*-LA to form a co-polymer.

1.3 CATALYST SELECTION

1.3.1 ROP

Polyesters are formed from cyclic esters via ROP reactions. ROP involves an organometallic catalyst with carefully selected ligands to fine-tune the steric and electronic properties of the metal complex. This allows control over the polymerisation process so that the characteristics of the polymer itself can be modified, in terms of properties such as M_n, PDI, monomer sequence, and stereoselectivity. The catalysis follows a coordination-insertion mechanism (**Figure 9**). This means the growing polymer chain remains coordinated to the metal centre after each monomer insertion. A metal centre that is electrophilic activates the carbonyl group on the cyclic ester by coordinating to it, which initiates the polymerisation. A nucleophilic ligand that is bound to the metal centre assists with the ring opening.[20]
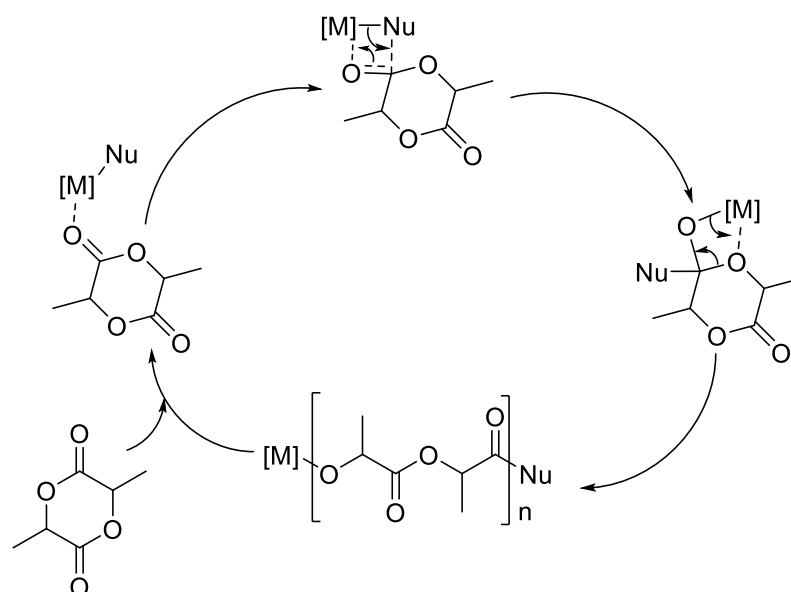
Figure 9: Coordination-insertion mechanism for ROP reaction with catalyst [M]-Nu, using LA as an example of a cyclic ester monomer. [M] = oxophilic metal centre with ancillary ligands e.g. Al, Y, La. Nu = nucleophilic initiating group e.g. NR_2. Figure adapted from ref.[20]

Using a monomer with chiral or pro-chiral centre(s) allows a polymer to be produced that demonstrates tacticity. As the polymer chain is propagated whilst it is bound to the metal centre, the catalyst can control the chirality of the next monomer to be incorporated in the

chain. This is known as chain-end stereocontrol mechanism (CEM), which subsequently allows for the tacticity of the polymer produced to be controlled.[20]

1.3.2 Catalyst Properties

A ligand in a metal complex should provide enough steric bulk so that complex dimerisation, ligand redistribution, and solvent ligation are prevented. However, the ligand needs to be compact enough that it does not render the catalyst inactive.[61] Multidentate bis(phenolate) (BP) ligands with an amino bridge are often used in stereoselective ROP catalysts. The general ligand design for synthesising a ROP catalyst (**Figure 10**) can be adapted to control stereoselectivity and activity. In particular, lanthanides and group 3 metals have been used for stereoselective ROP of racemic mixtures of cyclic esters. In the presence of a donor solvent, the metal complex forms a distorted octahedral structure, as it is 6 coordinate. The BP ligand binds to the metal via the O and N atoms in a meridional manner, with the bridge allowing the X donor group to bind at an axial position. The nucleophilic ligand (NZ_2 in **Figure 10**) binds trans to the N bridge atom, with tetrahydrofuran (THF) binding in the remaining axial position (Ln in **Figure 10**).[20]
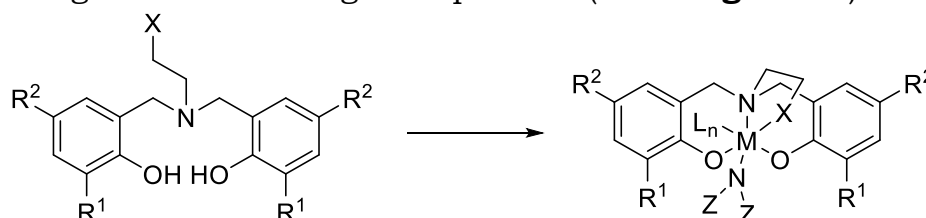
Figure 10: General ligand design for ROP catalysts and its coordination to a metal. M= metal; Z= SiRMe$_2$ where R=H/Me; R^1, R^2 = aryl substituents; X= OMe/NR$_2$ where R= Me/Et; L= donor solvent= THF where n=0/1. Figure adapted from ref.20

Kerton *et al.*[61] performed a screen of different complexes based on the structure in **Figure 10** for the ROP of ε-caprolactone (CL), where X was always a nitrogen based donor. They determined 3 main conclusions:

1. Steric demand of the ligand is significant.
    i. Bulky R^1 groups (e.g. tertiary butyl or tertiary pentyl) increased catalyst activity. Theoretically due to prevention

       of terminations, dimerisation of the complex, and protection of the active site.

    ii.   Having no R^1 group (i.e. no substituent) creates an inactive complex.

2. The type of nitrogen-based X donor is significant.

    i.   Secondary amines have lower conversion than tertiary, possibly due to competing NH activation. Pendant pyridyl donors also led to low activity, which was theorised to be due to strong donation to the metal centre.

3. Mid-sized rare earth metals (e.g. Y) have higher activity than larger and smaller metals.

    i.   Larger metal ions were theorised to facilitate terminations or dimerisations more readily than the mid-sized metal ions.

From these observations by Kerton *et al.*[61], a highly active catalyst with high monomer conversion and stereocontrol should be based on a mid-sized lanthanide or group 3 metal such as Y, with NR_2 as the X donor group, and bulky R^1 substituents. In addition, using NMe_2 as X as opposed to OMe led to higher levels of heterotacticity.[20] The X donor group is significant as nuclear magnetic resonance spectroscopy (NMR) studies have suggested that X remains coordinated to the metal throughout the ROP process.[62] Carpentier theorised that NR_2 encourages heterotacticity more so than OMe due to its greater steric bulk.[20] Further to Kertan's observations, it was determined that the bulkier the R^1 substituent, the higher the heterotacticity of PLA. In contrast, changing R^2 showed limited differences in heterotacticity. This supports the idea that the catalysis is under steric control and reinforces the CEM theory.[20]

By crowding the coordination sphere surrounding the metal centre, the orientation of the next monomer unit is subjected to a higher degree of influence from the propagating polymer chain.[20] There was also higher levels of heterotacticity observed for ROP of *rac*-LA when donor solvent

THF was used as opposed to non-donor solvent toluene. Bouyahyi *et al.*[56] used THF and toluene as solvents for ROP of *rac*-LA with a complex that had a BP ligand similar to that in **Figure 10**, with yttrium (III) as the metal centre. They found that in toluene, the PLA was atactic and in THF, it was heterotactic.[56] Marshall *et al.*[63] did a computational study using single-site β-diketiminate magnesium complex (**Figure 11**) as the catalyst. They found that the reaction proceeds via two main transition states, and whichever state has the highest energy, dictates the stereochemistry of the next monomer unit, and therefore the tacticity of the polymer. The donating solvent THF stabilises the transition states and balances the system entropically. They believed that similar features would apply to other LA polymerisation initiators.[63]
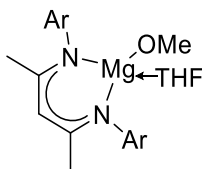
Figure 11: β-Diketiminate magnesium complex studied by Marshall *et al.*[63]

ROP of *rac*-BL follows similar trends to ROP of *rac*-LA, (for instance, syndiotacticity increases with decreasing ionic radii of the metal centre in the catalyst). A key difference between ROP of *rac*-BL and of *rac*-LA is that syndiotacticity is higher for PHB with non-donor solvents than donor solvents. Another key difference is the evidence for electronic as well steric effects to influence the tacticity of PHB. Bulky CMe_2tBu as R^1 (**Figure 12**) led to high heterotacticity in PLA with the probability of a racemic linkage (P_r) being 0.95. A racemic linkage refers to two monomer units bound together with opposite stereochemistry. However, for PHB, the P_r value is only 0.70. In contrast, the P_r values for PLA and PHB when using cumyl groups (CMe_2Ph, **Figure 12**) for R^1 were 0.91 for both. Adding to this evidence, by substituting a CF_3 group on the para position of the cumyl ring (**Figure 12**), the P_r value decreased to 0.83 for PHB.[20] This suggests that there are electronic as well as steric effects to consider when performing ROP with BL.
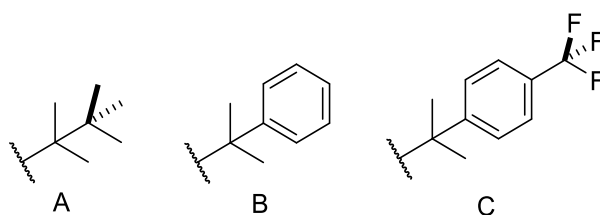
Figure 12: A = CMe$_2t$Bu; B = Cumyl = CMe$_2$Ph; C = p-CF$_3$ Cumyl.

Marshall *et al.*[63] suggested this was due to C−H⋯π interactions.[63] Bouyahyi *et al.*[56] identified C−H⋯π interactions between the CH$_2$ group in BL and the aryl R^1 substituents. They theorised that this could increase stereocontrol of the growing polymer chain.[56] This theory was evidenced with solid-state (NMR) and nuclear overhauser effect spectroscopy (NOESY) ^{1}H−^{1}H NMR of a complex where cumyl groups were the R^1 substituents (**Figure 13**). Close contact was confirmed between the cumyl rings and the BL CH$_2$ groups, instead of them being apart to minimise repulsive interactions between the polymer chain and the complex.[20]

IV-*trans-alkoxy/amino*
0 kcal.mol^{-1}

III-*trans-alkoxy/amino*
+9.8 kcal.mol^{-1}
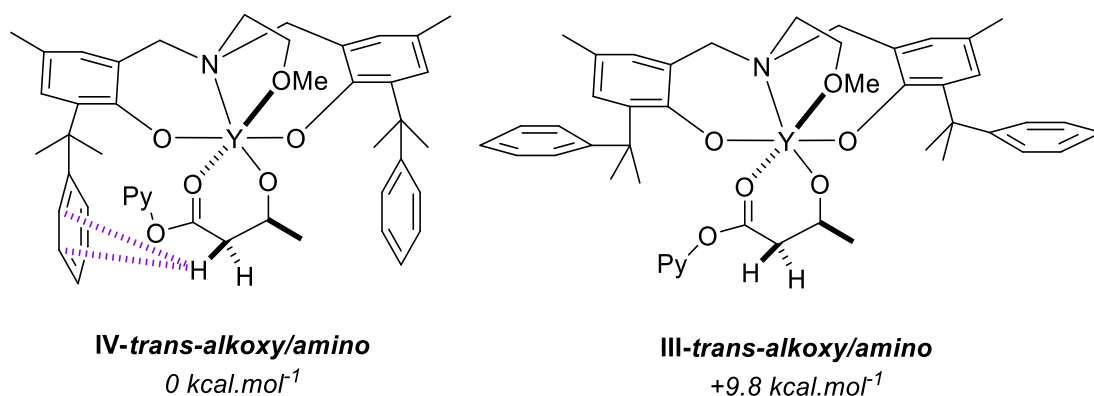
Figure 13: Schematic representation of two DFT-optimized model intermediates in the ROP of BL mediated by Y{ON(OMe)OCMe$_2$Ph,Me}(OR) species, showing C–H⋯π interactions (relative computed energies; P stands for the polymeryl chain). Where DFT is density functional theory calculations. Figure and caption adapted from ref.20

In summary, medium sized rare earth metals (such as yttrium) have proven to be the best choice for the metal centre as they are more active than the larger metals. X is often either a methoxy or tertiary amine group. The oxygen/nitrogen remains coordinated to the metal

throughout the ROP process. Having nitrogen coordinated to the metal offers higher activity and in the case of synthesising PLA, encourages heterotacticity in the polymer. Cumyl groups as R^1 and R^2 offer enough steric bulk, as well as the desired electronic effects for producing syndiotactic PHB. Performing the reaction in a donor solvent such as THF also encourages heterotacticity in PLA. Generally, if a catalyst is good at producing heterotactic PLA, then it is good at producing syndiotactic PHB.[20]

1.3.3 Catalyst Design

A catalyst (**1**) was developed in the Platel group for the copolymerisation of LA and BL (**Figure 14**). It produces a copolymer with a composition that reflects the monomer feedstock. It has bulky cumyl substituents as R^1 and R^2, dimethylamine as the X donor group to coordinate to the metal, and yttrium (III) as the metal centre. Therefore, this catalyst is highly active. Additionally, it should produce a copolymer where the LA monomer units are heterotactic with respect to each other and the BL monomer units are syndiotactic with respect to each other. This is due to the bulky coordination sphere provided by the ligand, as discussed earlier in section 1.3.2.

1
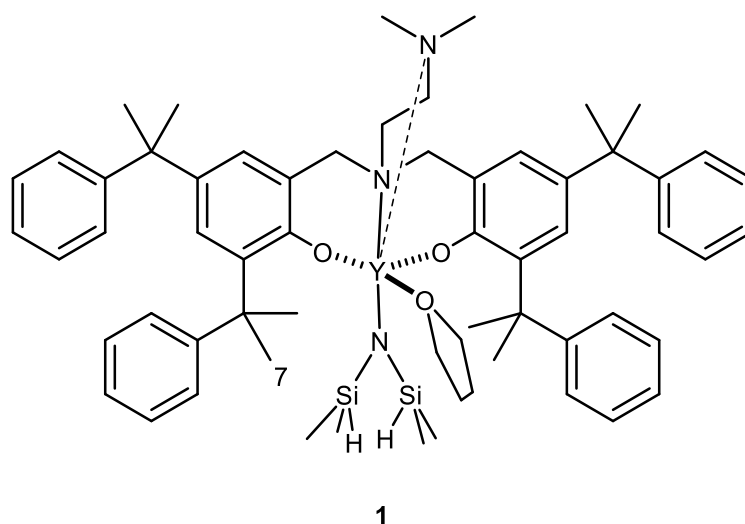
Figure 14: Catalyst to be used for co-polymerisation of LA and BL.

1.4 AIMS

The overall aim of this project was to investigate a copolymer for its potential to replace PE in single-use coffee cups. PLA and PHB were chosen to copolymerise as they were thought to have a complementary combination of properties for this desired purpose. In addition, they are both bio-based. Copolymers were synthesised and analysed to determine the T_m and T_g of the polymers using DSC. The polymers with a T_m greater than 100 °C were subjected to further testing. The copolymers were made into films and subjected to water permeability tests to further investigate their potential to be used to coat paper intended for use in single-use beverage cups.

1.5 CHARACTERISATION

1.5.1 DSC

In differential scanning calorimetry (DSC), a sample is heated in a crucible at the same time as a reference (an empty crucible) within the same chamber (**Figure 15**). Samples are generally heated over a given temperature range at a controlled rate (e.g. 10 °C/min) and then cooled at a controlled rate. The difference in thermal energy required to increase the temperature of both crucibles by the same amount is measured. Upon heating/cooling, the enthalpy and/or heat capacity of a sample can change (e.g. during a phase transition) and the temperature this occurs at can be identified using DSC. This method is quick; however, the sample cannot easily be retrieved once it is sealed in the crucible. Although, the exact same sample can be subjected to
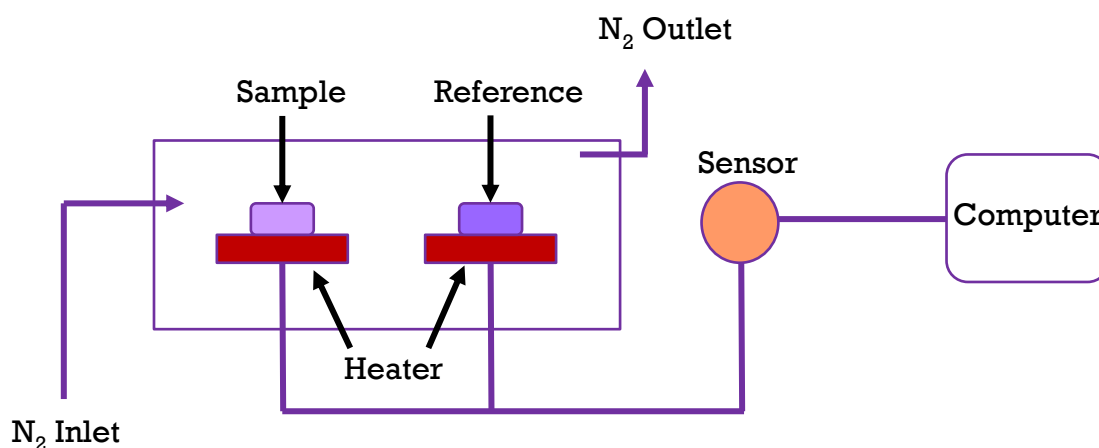
Figure 15: DSC diagram adapted from ref.64

further DSC analysis.[64]

DSC is commonly used to characterise the thermal behaviours of polymers, including semi-crystalline and modified polymers. DSC can, directly measure the T_g, T_m, and temperature of crystallisation (T_c), as well as the associated enthalpies. Indirectly, the w_c of the sample can be calculated.[64]

1.5.2 TGA

In thermogravimetric analysis (TGA), the mass of a sample is recorded whilst the temperature is increased (**Figure 16**). This allows the thermal

decomposition behaviour of the substance to be studied. The T_o and T_{max} can be determined, as well as information on the thermal decomposition process itself. Like with DSC, the heating rate of the sample is controlled, and the sample is sealed in a crucible. However, a hole is pierced in the lid of the crucible to allow gases from decomposition to escape, and hence allow for a change in mass. The sample can also be held at certain temperatures and the rate of heating can be changed throughout the experiment if the programmer wishes. The mass balance used in the machine is very sensitive; mass changes as little as 0.0001 g can be detected. Additionally, the flow of gas into the furnace (typically air, nitrogen or argon) is controlled at a set flow rate determined by the programmer.[64]
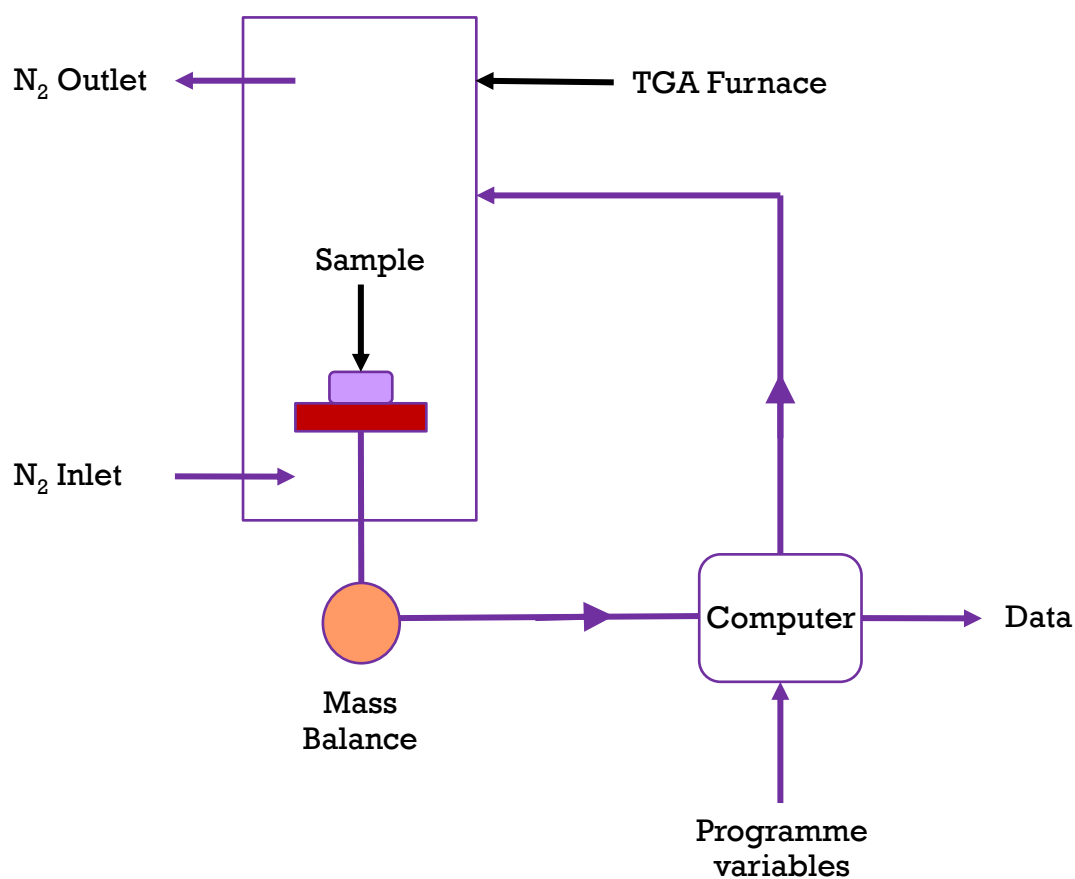
Figure 16: TGA diagram adapted from ref.64

TGA can be useful for determining the decomposition process of the polymer and the order of this reaction. It can also show at what

temperature(s) mass is lost which can be important if the polymer is desired to be used in a consumer product. However, this technique is destructive and the sample cannot be retrieved or the same sample be re-run.[64]

1.5.3 GPC

Gel permeation chromatography (GPC, also known as size-exclusion chromatography) is used to determine the molecular weight(s) of a polymer sample, as well as the polydispersity index (PDI). This is a measure of the range of molecular weights present where a PDI value of 1.0 indicates the sample is uniform (i.e. all the polymer chains are the same length) and the higher the value climbs, the less uniform the sample.

The polymer sample is injected into a solvent stream (**Figure 17**), that has been degassed to prevent damage to the column. The sample flows into a column containing a stationary phase that is highly porous, such as silica beads or a polymer gel.[64,55] The smaller the molecule, the more pores it can diffuse into, thus taking longer to elute than a larger molecule that cannot diffuse into as many pores.[55] This means that retention time is inversely proportional to the size of the molecules.[64] The molecules are detected in the eluent upon leaving the column using refractive index, light scattering, and/or viscometer detectors. Using all three detectors is known as triple detection GPC.[65]
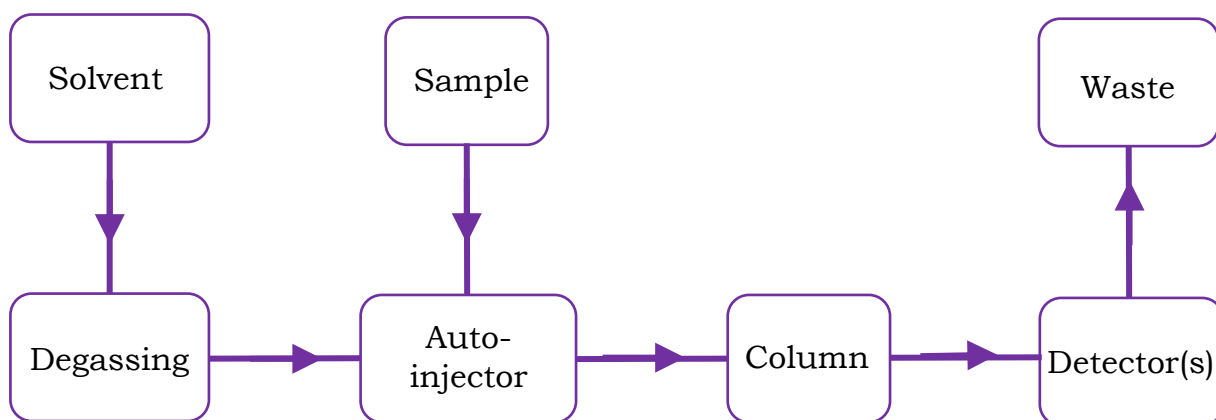
Figure 17: Basic GPC diagram.

The refractive index detector is calibrated with polymer samples of known relative molecular mass (RMM) prior to running the unknown sample. Typically, polystyrene is used as a standard, however this can cause some issues as the polymer standards should ideally be the same polymer or polymer type as the polymer being analysed.[55] The light scattering detector measures the molecular weights within the sample independently of prepared polymer standards. The viscometer detector can measure molecular weight as a function of intrinsic viscosity of the sample. It can also provide structural information abou t the polymer, such as whether it is branched or linear.[65]

GPC is considered a relatively quick method to determine PDI values. It can be used quickly in industry to check quality of batches of materials as two chromatograms can be easily compared. It is important to note that the instrument is sensitive to different conditions such as solvent, temperature and mechanical instability. Additionally, the polymer samples need to be soluble to be tested.[64]

1.5.4 PXRD

Powder X-ray diffraction (PXRD) is used to analyse the w_c of a sample or to gain information about the crystalline nature of a sample (e.g. unit cell parameters, atomic spacing). Uniform X-rays are directed at a sample by an X-ray source (**Figure 18**). When an incident ray has the correct wavelength to satisfy Bragg's Law, there is constructive interference and an X-ray is diffracted to the detector. The wavelength of the incident X-ray and the angle at which this diffraction occurs, is related to the lattice spacing in the crystal. The diffracted X-rays are counted by the detector, which can be plotted against 2θ.[66] The narrow peaks on the spectrum correspond to the crystalline regions of the sample, and wide peaks correspond to the amorphous regions of the sample.[67]
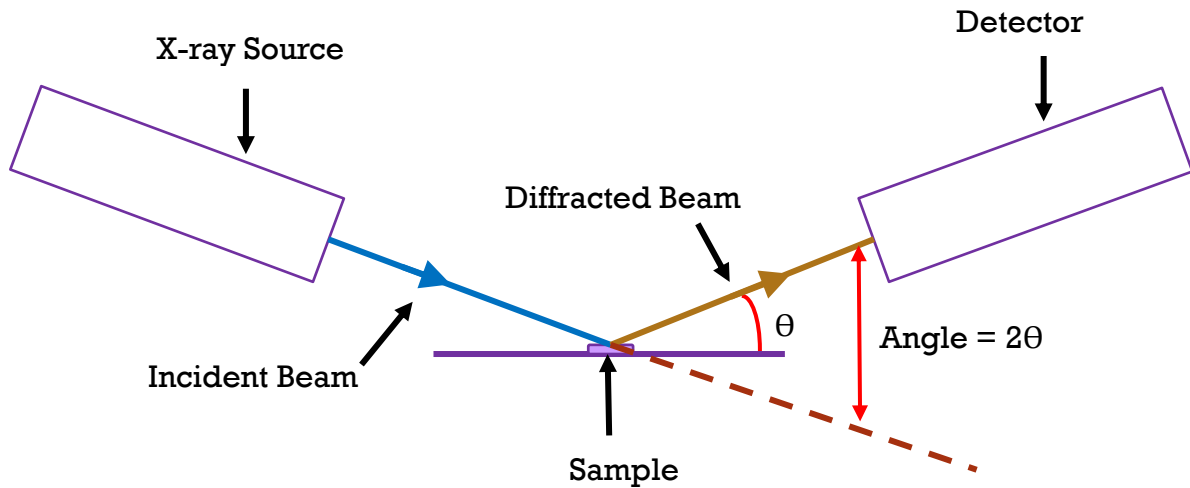
Figure 18: A diagram of the powder x-ray diffractometer.

For this project, PXRD was used to determine the w_c of the polymer film samples (see section 2.3.1).

1.5.5 SEM

Scanning electron microscopy (SEM) is similar to a light microscope in that it magnifies an object to form a close-up image; however, the main difference is that SEM uses electrons instead of light to generate the image. A metal filament is heated to generate electrons in the electron gun (**Figure 19**) to form the electron beam. The beam passes through an electromagnetic lens, which focuses the electrons on the sample. Upon reaching the sample, the electrons can be backscattered or create secondary electrons which are collected by their respective detectors. The detectors relay this information back to a computer and an image is generated.[68]

To analyse films made from PHB, Bergstrand *et al.* sputter coated the sample with gold. They looked at the films using a magnification of 5000 at 3 kV. They also performed elemental analysis using energy dispersive X-ray spectrometry (EDX).[69] Shojaeiarani *et al.* analysed PLA films using SEM at a magnification of 100 at 10.0 kV. The samples were bound to aluminium mounts using adhesive carbon. They were then coated in conductive carbon using a high vacuum evaporative coater.[70] Abdelwahab *et al.* used SEM to analyse films made from PLA/PHB blend. First, they coated the samples in gold/palladium in a sputter

coater to view them using a 2 kV voltage.[71] These papers were used to determine that the samples in this project should be coated in gold, before being analysed using a low voltage to prevent damage to the specimens.
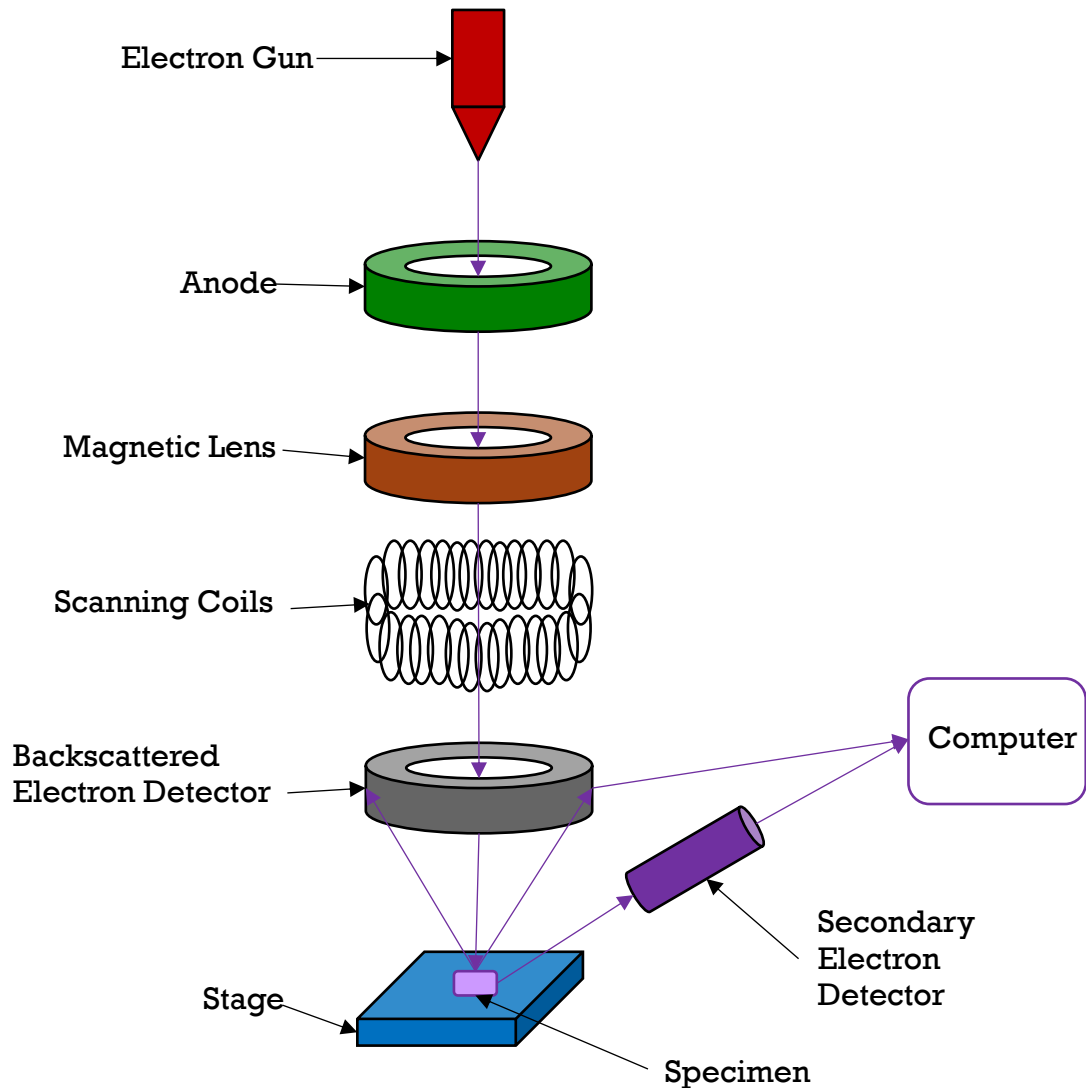
Figure 19: A basic diagram of how the SEM works, where the purple arrows represent electron beams. Figure adapted from ref.68

2　RESULTS AND DISCUSSION

2.1　CATALYST SYNTHESIS

2.1.1 Ligand

The chosen ligand was 2,2'-[[[2-(dimethylamino)ethyl]imino] bis(methylene)]bis[4,6-bis(1-methyl-1-phenylethyl)-phenol, **5**. The yield obtained was 80.0%, which was an improvement on the reported yield in the literature of 67%.[72] The desired product was confirmed by NMR analysis. The ^{1}H NMR (**Figure 20**) showed the product was reasonably pure. The ^{13}C NMR also confirmed the ligand had been successfully synthesised. Both spectra were assigned in agreement with Zhu *et al.*[72] and Reiter *et al.*[73] The absence of aldehyde protons from formaldehyde and amine protons from *N,N*-dimethylethylenediamine, combined with the presence of a new peak for protons 4 confirm the transformation of the starting materials to the product.
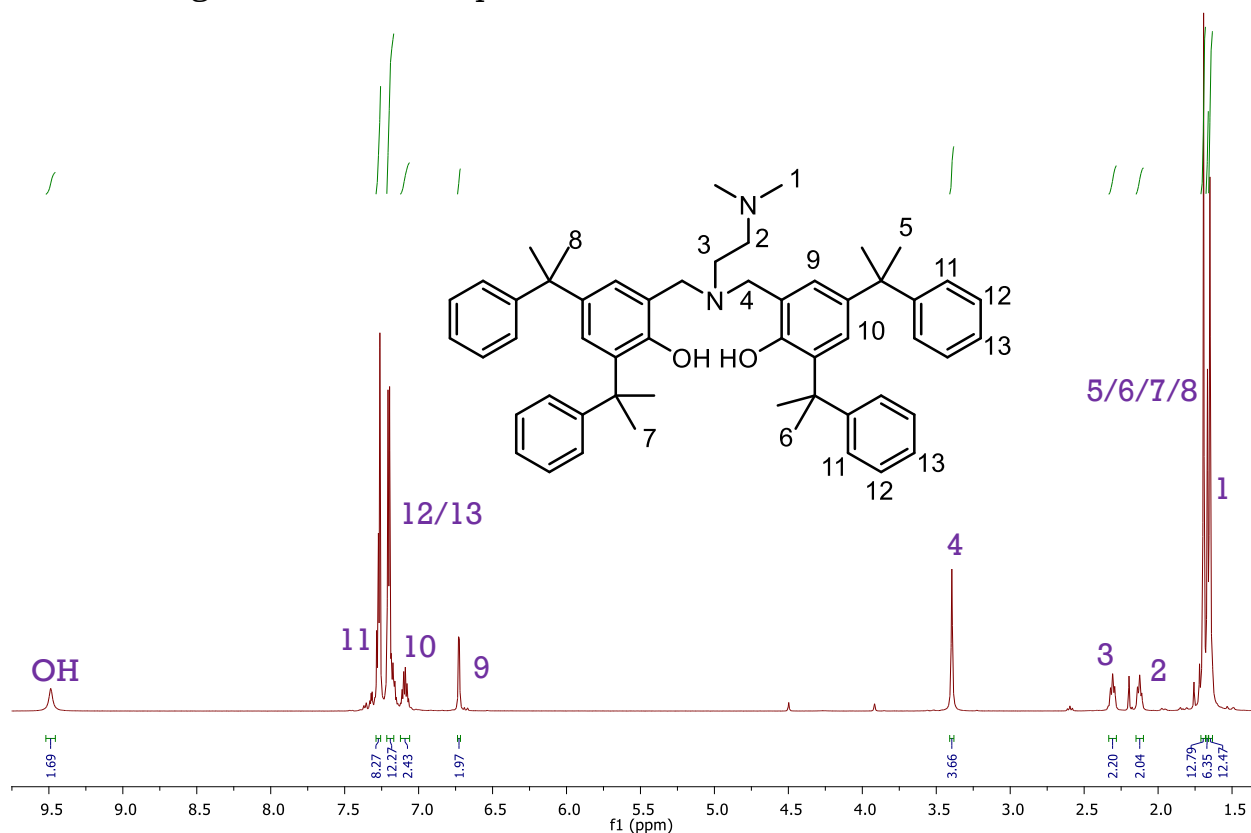
Figure 20: ^{1}H NMR and assignment of the ligand, **5**, where the numbers correspond to each proton environment.

2.1.2 Catalyst

The catalyst (**1**) was synthesised in 64% yield. The structure of the catalyst was confirmed to have been synthesised by ^{1}H, ^{13}C NMR analysis. Including [1]H-^{1}H correlated spectroscopy (COSY), heteronuclear single quantum coherence (HSQC), and NOESY.

All protons were assigned numbers using the same system as was used for the ligand (**Figure 20**). SiMe, THF, and Si-H are new proton environments that were not present in the ligand. The aliphatic region was assigned as observed in **Figure 21**. Protons environments 5, 6, 7, and 8 have different chemical shifts in the catalyst compared to the ligand. In the ligand, these proton environments were observed as two peaks, which integrated to twelve protons each at almost identical chemical shifts at approximately 1.6 ppm. In the catalyst, these proton environments were observed as two peaks at almost identical chemical shifts at approximately 1.6 ppm. These integrated to six protons each, which corresponded to proton environments 5 and 6. Proton environments 6 and 7 shifted downfield to approximately 1.7 and 2.0 ppm. The methyl groups with proton environments 6 and 7 could either be orientated towards the centre of the metal complex, or away from the centre of the metal complex. This led to one of the methyl groups in proton environment 6 and one of the methyl groups in proton environment 7 being in the same chemical environment as each other, as they both are orientated towards the metal centre. The other pair of methyl groups with proton environments 6 and 7 are in a separate environment as they point away from the metal centre. This was confirmed by NOESY.

The protons in environment 2 and 3 have shifted downfield compared to the ligand spectrum. This is due to the deshielding effects of the lone pairs on the nitrogen atoms donating to the yttrium metal centre. In addition, they have overlapped with the hexane CH_2 multiplet, confirmed by two distinct CH_2 proton environments on the HSQC spectrum.

The protons in environment 4 have split into two doublets, which is in contrast to the singlet observed in the ligand spectrum. One doublet has remained at a chemical shift of approximately 3.3 ppm, as observed in the ligand. However, the other doublet was observed upfield at approximately 2.3 ppm. As the ligand has chelated to the yttrium, one proton in environment 4 is orientated more towards the centre of the metal complex than the other. This leads to one of the two protons in each environment being more shielded than the other, so they are no longer equivalent. They are diastereotopic, therefore the two protons couple to each other even though they are bound to the same carbon. As a result, they were observed as two doublets. This was confirmed by COSY.

The aromatic region was assigned as observed in **Figure 22**. The protons in environments 9 and 10 both shifted downfield compared to the chemical shifts observed in the ligand spectrum. The protons in environment 10 shifted downfield by almost 1 ppm. The protons in environments 12 and 13 were observed at slightly different chemical shifts in the catalyst spectrum compared to the ligand spectrum. In the catalyst spectrum, these two proton environments are distinguishable; however, they are indistinguishable in the ligand spectrum.
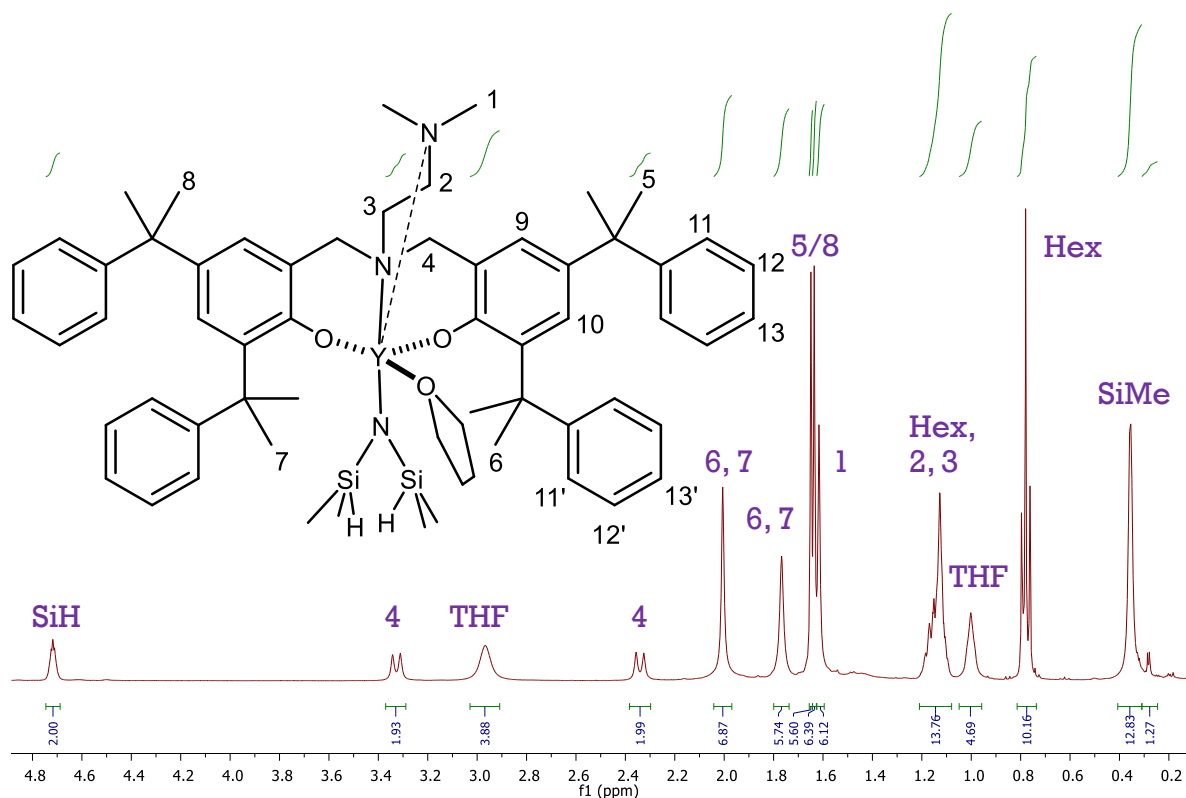
Figure 21: Aliphatic region of ^{1}H NMR spectra for the catalyst, **1**.
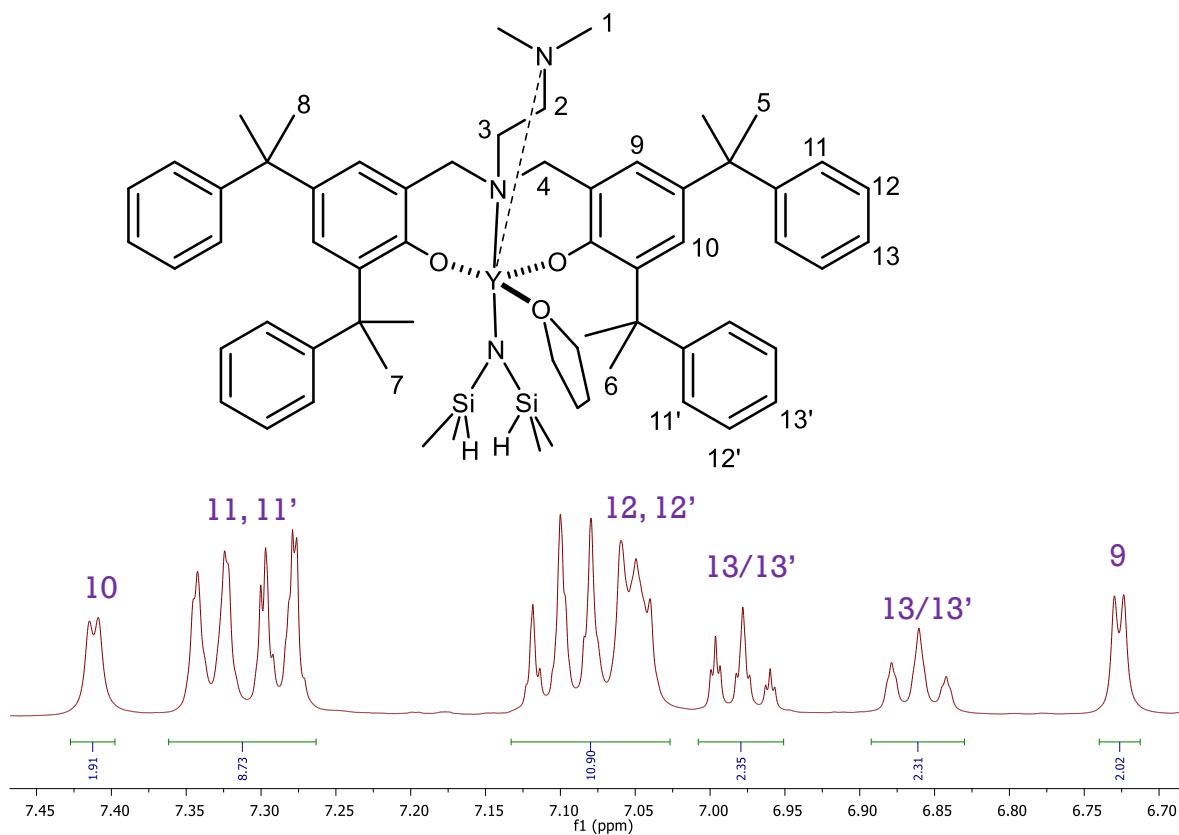
Figure 22: Aromatic region of ^{1}H NMR spectra for the catalyst, **1**.

2.2 POLYMERS

Polymers were synthesised using various monomer ratios (**Table 1**). The yields obtained varied between 51-71%. The yields varied slightly due to not all the BL monomer being converted in the reaction (see **Table 2**). Also, some of the product could have been lost during the recrystallisation step.

Table 1: Polymerisation reactions performed. Catalyst: monomer ratio was 1:800. All reactions carried out with a total of 16 mmol of monomer.

Entry	Molar Ratios		Yield (%)
	BL	LA	
P1	50	50	53
P2	60	40	51
P3	70	30	71
P4	75	25	62
P5	80	20	61
P6	85	15	63
P7	90	10	64
P8	95	5	62
P9	100	0	53
P10	0	100	51

Throughout the rest of this thesis, the polymers will be referred to as the entries in **Table 1**.

2.2.1 ^{1}H NMR

Taking **P1** as an example, ^{1}H NMR assignment along with calculations for monomer conversion, copolymer composition and percentage of hetero-linkages will be shown.
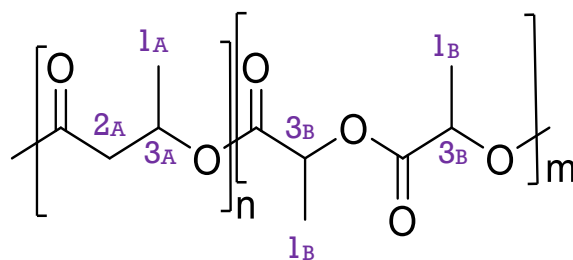
Figure 23: BL/LA copolymer where the 1, 2, and 3 are CH_3, CH_2, and CH environments respectively. A and B correspond to BL and LA protons respectively.

2.2.1.1 Assignment

^{1}H NMR spectra of all the polymers were successfully assigned. An example using **P1** is shown in **Figure 24**. Yttrium was found to be present in the polymer samples as evidenced during EDX analysis (see section 2.3.2). The yttrium catalyst would have decomposed once the reaction mixture was exposed to air during quenching, although it will still exist as a complex. It is possible that the yttrium coordinated to THF after decomposition, hence a THF peak being present in the polymer products.
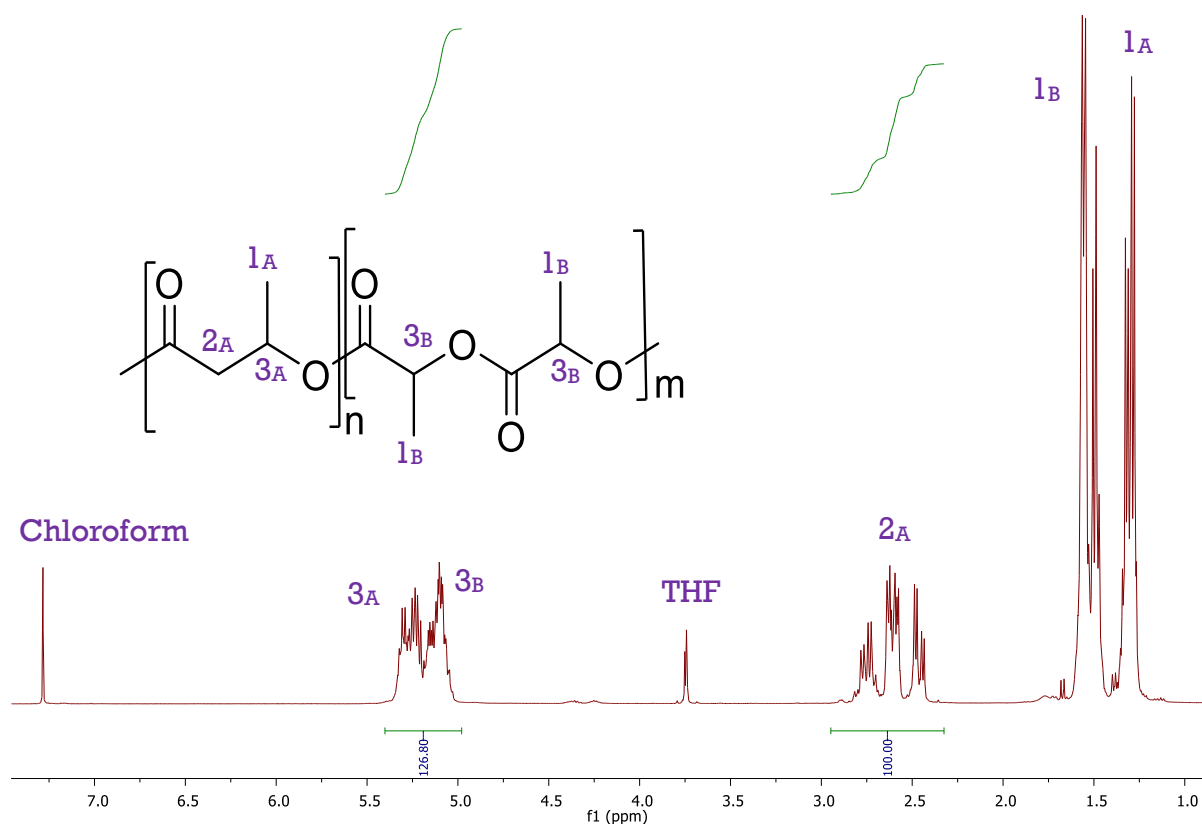
Figure 24: ^{1}H NMR of pure **P1** to show the proton environments of BL/LA copolymers.

2.2.1.2 Monomer Conversion

^{1}H NMR of crude polymer was used to determine the extent of monomer conversion into polymer. LA has a distinctive quartet peak at around 5.0-5.1 ppm. In all the polymers, LA had 100% conversion as this quartet was not observed. The BL monomer had a characteristic doublet of doublets peak between 3.0-3.7 ppm. By integrating this peak, and integrating the CH_2 region of the polymer peaks (that only protons

belonging to PHB give rise to), monomer conversion of BL can be determined. By setting the total integral to 100, the integral for the polymeric region equates to the percentage conversion for the BL monomer, as shown in **Figure 25**.
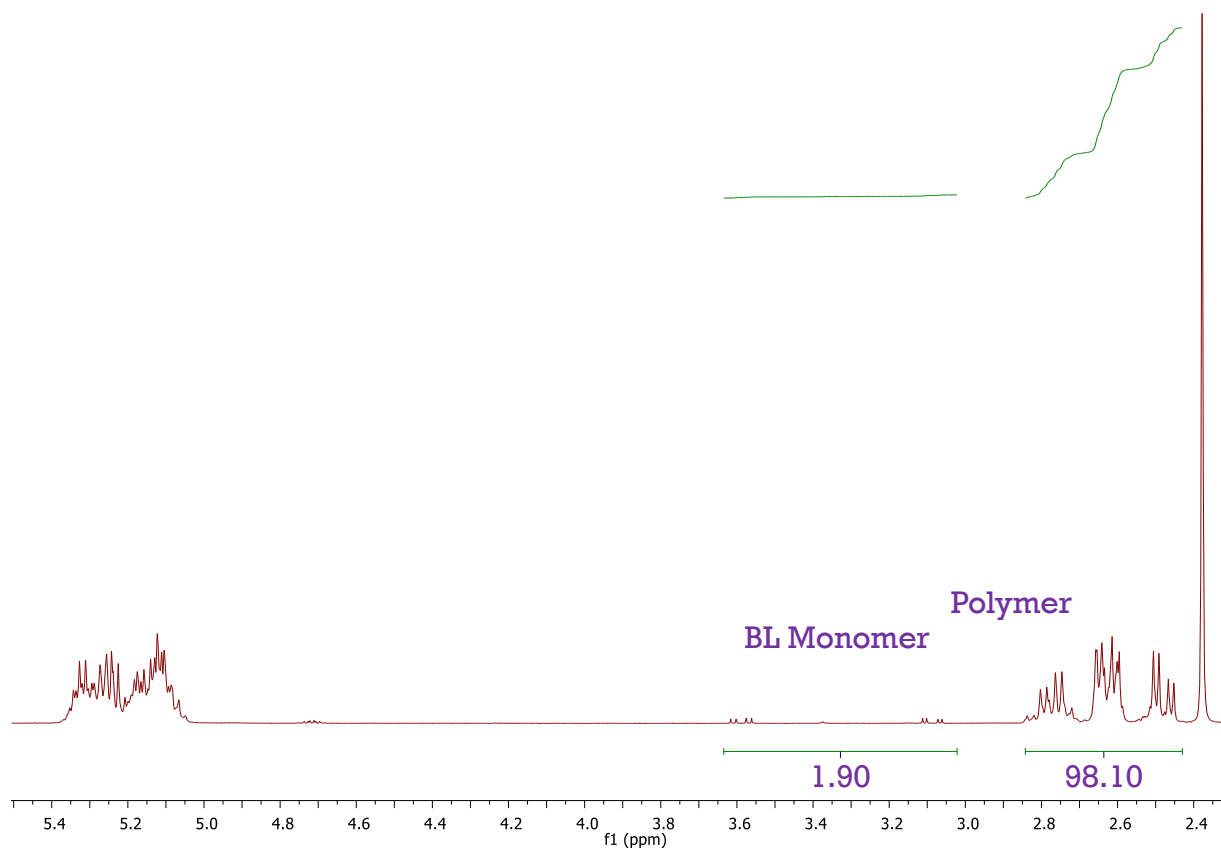
Figure 25: ^{1}H NMR spectrum of crude **P1** to show the extent monomer conversion of BL and LA.

2.2.1.3 Copolymer Composition

Using the ^{1}H NMR spectra from the pure copolymer, the composition can be calculated. **Figure 26** shows the pure ^{1}H NMR spectrum for **P1**. The CH and CH$_2$ regions have been identified and are associated with protons 3 and 2 respectively (**Figure 23**). First, the CH$_2$ region (associated only with 2 protons from BL and assuming 50 monomer units of BL) was integrated to 100. Then, the CH region was integrated. 50 was subtracted from the CH region integral as this represents the 50 protons from the 50 monomer units of BL. This value was then divided by 2, as there are 2 CH environments per LA monomer unit. This value was denoted as x. x Was then divided by $x+50$ to obtain the percentage

of LA in the copolymer (%LA) (**Equation 1**). A worked example for **P1** is shown in **Equation 2**.

Equation 1: Calculation for finding the percentage of LA in a copolymer.

$$\frac{1}{2}(CH - 50) = x \quad \frac{x}{x+50} \times 100 = LA\%$$

Equation 2: Worked example using **Figure 26**.

$$\frac{1}{2}(126.8 - 50) = 38.4 \quad \frac{38.4}{88.4} \times 100 = 44\%$$

CH Region, 3 CH_2 Region, 2

126.8   100.0
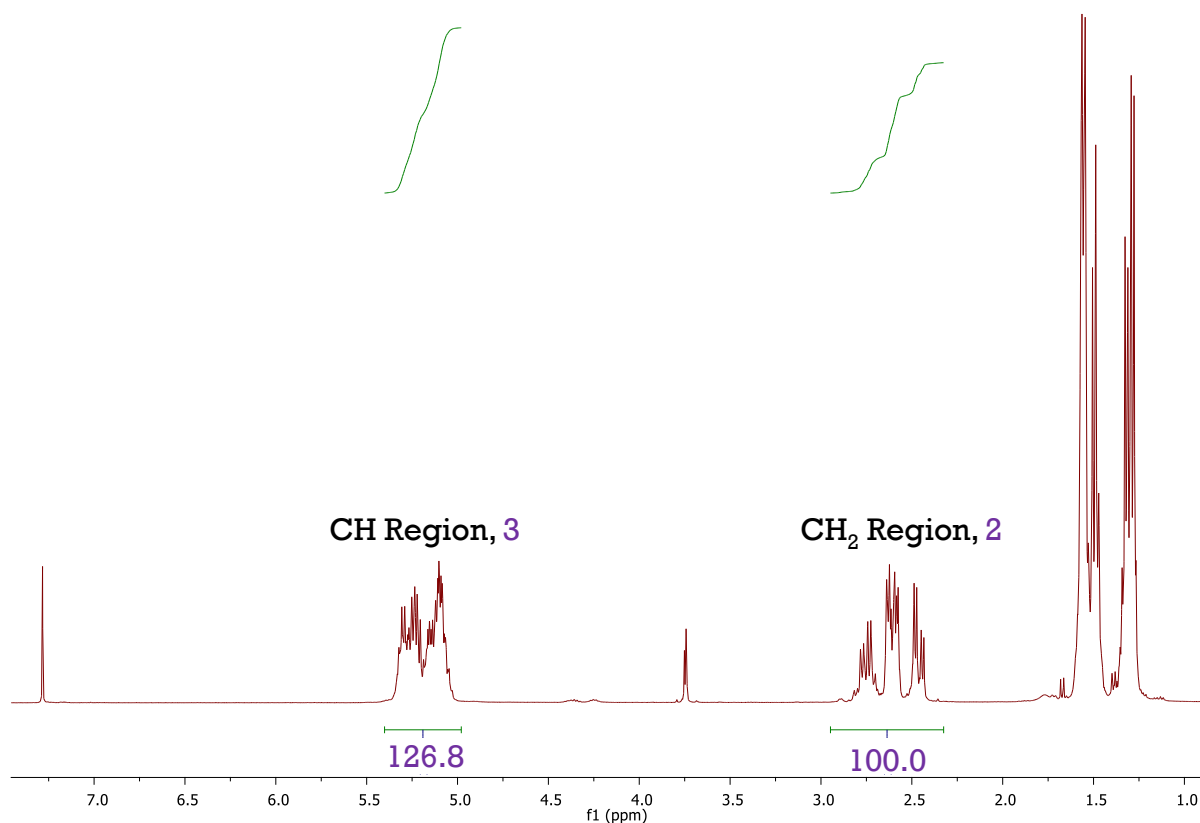
Figure 26: ^{1}H NMR spectrum of pure **P1** sample.

2.2.1.4 Percentage of Hetero-linkages

A hetero-linkage is a bond between neighbouring BL and LA monomers, whereas a homo-linkage is a bond between neighbouring BL monomers or neighbouring LA monomers.[43] The percentage of hetero-linkages for each polymer was calculated using the method reported by Fagerland *et al.*[43] In the CH_2 region, there are 3 different peaks. These peaks have

been labelled X, Y, Z in **Figure 27**. Peak X and half of peak Y is related to the hetero-linkages in the polymer. The other half of peak Y and peak Z are related to the homo-linkages. By integrating this region to 100 and doubling the integral of peak X, an estimate for the percentage of hetero-linkages can be found. In the case of **P1**, after integrating the CH_2 region to 100, peak X had an integral value of 27.87. Double this value was 55.74 so the percentage of hetero-linkages in this polymer was 56%.
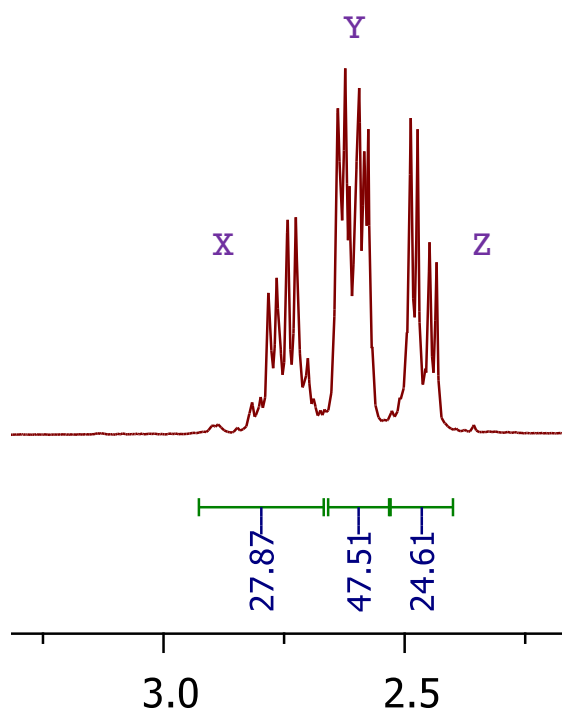
Figure 27: CH_2 region of the ^1H NMR spectrum for the pure **P1** sample.

2.2.1.5 Summary of ^1H NMR Data

The polymer composition reflects the monomer feed ratio consistently with the greatest difference being 6% for **P1** (**Table 2**) and the second greatest difference being 2%. This demonstrated that the catalyst was working effectively to produce a polymer with a composition that reflects the monomer feed ratio. In addition, the catalyst was shown to be working effectively by the conversion percentages of the 2 monomers. LA was always 100% converted and the lowest conversion of BL was 89%, with half of the reactions showing a conversion of 95% or higher.

The percentage of hetero-linkages decreased with increasing percentage composition of BL in the polymer (%BL). This is expected as there is less possibility of a hetero-linkage being formed with decreasing %LA. The percentage of hetero-linkages was approximately 1.6 times the %LA for samples **P1**-**P7**. This shows that the monomers are linked in a random order in the polymer, as opposed to alternating or as two blocks.

Table 2: Summary of the polymer compositions, percentage conversions, and percentages of hetero-linkages.

Polymer	Monomer Feed Ratios		Polymer Composition		Conversion		Hetero-linkages (%)
	BL	LA	BL (%)	LA (%)	BL (%)	LA (%)	
P1	50	50	56	44	98	100	56
P2	60	40	62	38	94	100	47
P3	70	30	72	28	99	100	35
P4	75	25	74	26	94	100	34
P5	80	20	80	20	98	100	25
P6	85	15	84	16	93	100	21
P7	90	10	88	12	89	100	17
P8	95	5	96	4	90	100	14
P9	100	0	100	n/a	95	n/a	n/a
P10	0	100	n/a	100	n/a	100	n/a

2.2.2 DSC

DSC analysis was performed on all 10 polymers. From the thermograms, the T_g, T_c and T_m were determined and averaged over 3 runs (**Table 3**). An example is shown in **Figure 28**, which is the DSC thermogram of **P5**. The thermograms were orientated so endotherms are peaks and exotherms are troughs. A melting peak was identified in each run (orange box). This peak in the 1st run (black line) was visibly different to the peaks in the 2nd and 3rd heating scans (blue and purple lines respectively). The T_m value was taken as the top of the peak and was similar across all 3 heating scans. However, the enthalpy of melting (ΔH_m), which was the normalised integral of the melting peak, was found to be 11-37% higher in the 1st run than the 2nd and 3rd runs (which were similar values to each other) for samples **P1-P9**. Therefore, this value was averaged using only runs 2 and 3. This finding was theoretically

40

due to the thermal history of the polymer. When the polymer was synthesised, it was crystallised from solution. After the first melt, the polymer sample was crystallised from the melt. So, the ΔH_m from the first heating cycle was different from the heating cycle for runs 2 and 3. This theory is also evidenced by the enthalpy of crystallisation (ΔH_c) being only 0-4% different across all 3 runs for each of the samples **P1**-**P9**, as the thermal history of the sample would have been removed. Therefore, the final ΔH_c value was an average of all 3 runs. The T_c value (pink box) was taken as the bottom of the trough and was similar across all 3 cooling scans. Sample **P10** was completely amorphous (as confirmed by PXRD, see section 2.3.1) so no melting or crystallisation peaks were observed. The T_g values (grey box) were taken as the inflection point of the curve on the cooling scans.
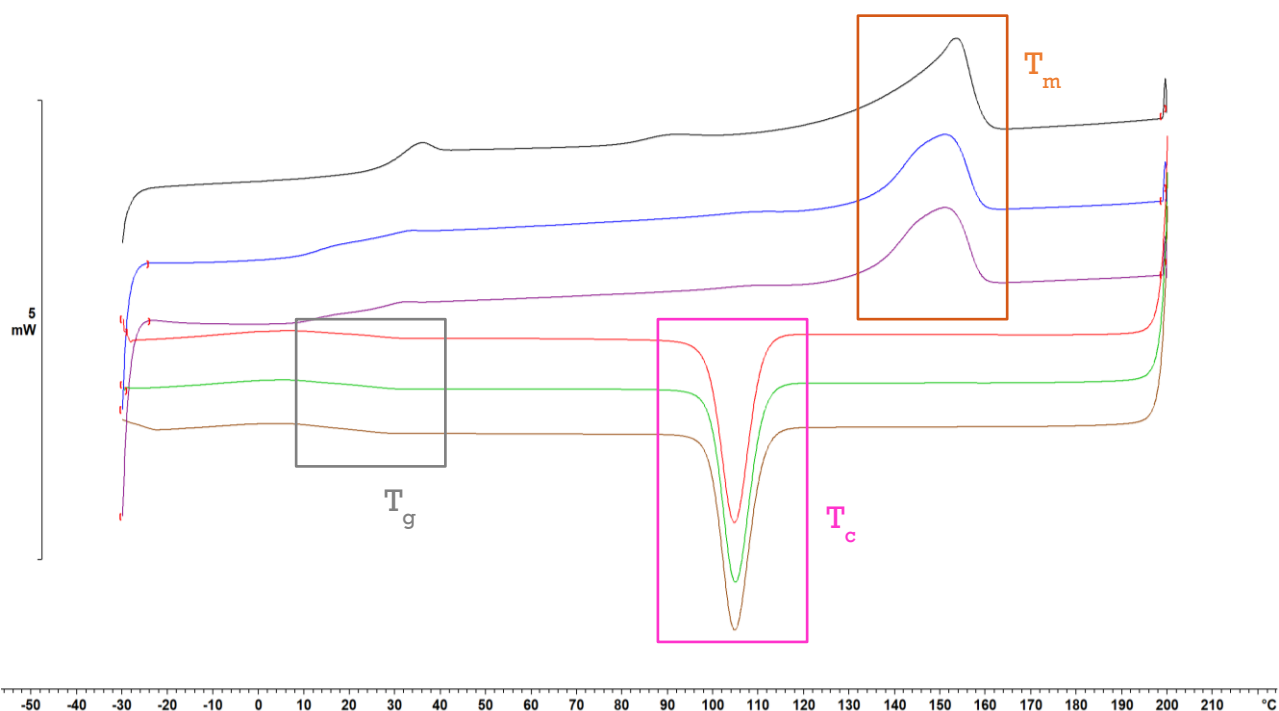
Figure 28: DSC thermogram of **P5**. Where the 1st, 2nd, and 3rd heating scans are coloured black, blue, and purple respectively. The 1st, 2nd, and 3rd cooling scans are coloured red, green, and brown respectively.

From the averaged enthalpies, the w_c was calculated using **Equation 3** for homopolymers **P9** and **P10**. **Equation 3** and **Equation 4** were combined to create **Equation 5**, which was used to calculate w_c for the copolymers. The enthalpy of melting for a 100% crystalline samples of the polymers ($\Delta H_m^{\ominus}$) was found in the literature to be 146.6 J/g[74] for PHB. The PLA that was synthesised was 100% amorphous, so had a maximum crystallinity value of 0%.

Equation 3: Equation used to calculate w_c from the DSC data for homopolymers, adapted from ref. 75.

$$w_c = \frac{-\Delta H_c}{\Delta H_m{}^{\ominus}} \times 100$$

Equation 4: Equation to calculate the average $\Delta H_m^{\ominus}$ for the copolymers, adapted from ref. 76.

$$\Delta H_m{}^{\ominus} = \Delta H_m{}^{\ominus} BL \times \%BL$$

Equation 5: An adaption of **Equation 3** and **Equation 4** to calculate the w_c for copolymers.

$$w_c = \frac{-\Delta H_c}{\Delta H_m{}^{\ominus} BL \times \%BL} \times 100$$

Table 3: The thermal data of the polymer samples as determined by DSC.

Polymer	Mass (mg)	T_g (°C)	T_m (°C)	T_c (°C)	ΔH_m (J/g)	ΔH_c (J/g)	W_c (%)
P1	5.00	20.60	144.66	81.50	10.21	-10.86	13
P2	3.40	25.25	148.38	92.64	11.9	-13.25	15
P3	6.08	20.41	149.61	94.78	16.67	-18.76	18
P4	5.00	12.20	148.59	104.37	18.84	-22.68	20
P5	3.53	24.37	151.73	105.01	22.25	-27.41	23
P6	8.16	10.90	151.10	104.40	25.74	-30.62	24
P7	7.32	10.30	152.15	108.71	25.77	-32.53	25
P8	6.54	7.35	151.77	112.16	30.12	-38.04	27
P9	7.38	1.15	154.52	119.40	33.98	-44.39	29
P10	3.99	41.32	n/a	n/a	n/a	n/a	0

By plotting the T_g values against the %BL in the polymer (**Figure 29**), as the %BL was increased in the copolymer, the T_g decreased with **P9** having the lowest T_g value and **P10** having the highest. There was a trend between the %BL in the polymer and the T_g, however this is not a perfect trend as the T_g values did not correlate well enough to generate a line of best fit between the **P10** T_g and the **P9** T_g values. The poor trend could be partially attributed to the inconsistency in the mass of the sample submitted for analysis. Similarly, by plotting the T_m values against the %BL in the polymer (**Figure 30**), a trend could be observed. Although, it was opposite of the observed trend with the T_g values. The T_m increased as the %BL in the polymer increased. **P9** had the highest observed T_m. The trend correlated better with the line of best fit than observed with the T_g values. Additionally, it was observed that as the T_g decreases, the T_m increases so as the %BL is increased in the polymer, the difference between the T_g and T_m increases. Importantly, samples **P1-P8** melt at a temperature significantly higher than the boiling point of water, which is essential if they are to be used to line single-use coffee cups. In addition, the w_c increased as the %BL in the polymers increased (**Figure 31**), almost linearly. The data points for polymers **P1-P9** closely follow the line of best fit, which was extrapolated to estimate that at 20% polymer composition of BL, or less, the w_c would be 0%.
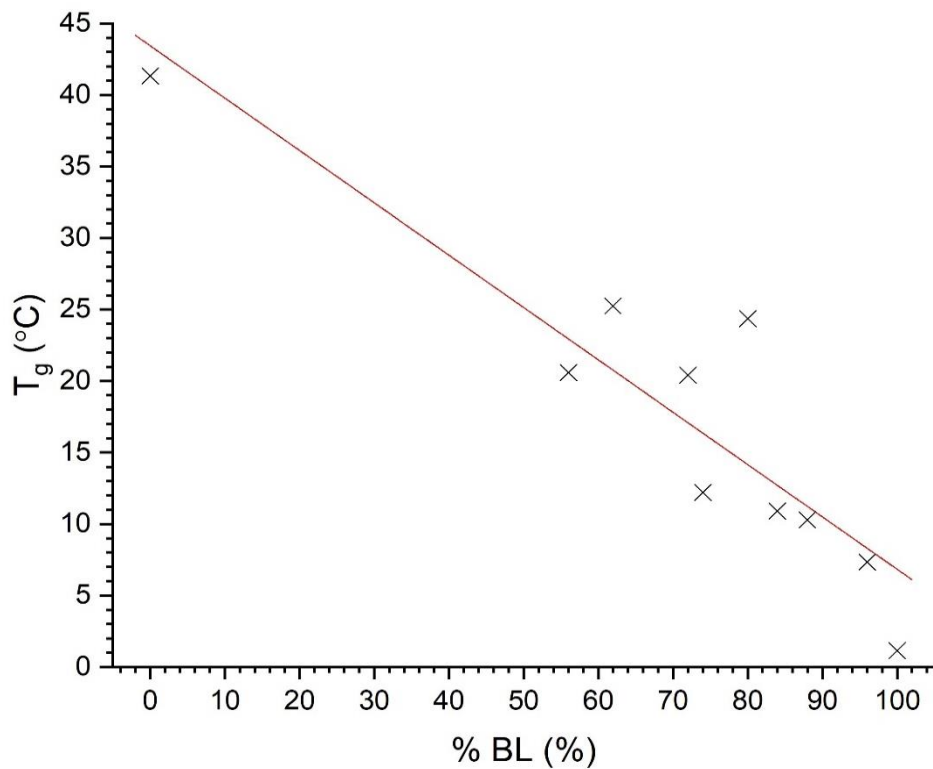
Figure 29: Plot of T_g vs %BL. Line of best fit generated with equation:
$$T = -0.366\%BL + 43.4.$$
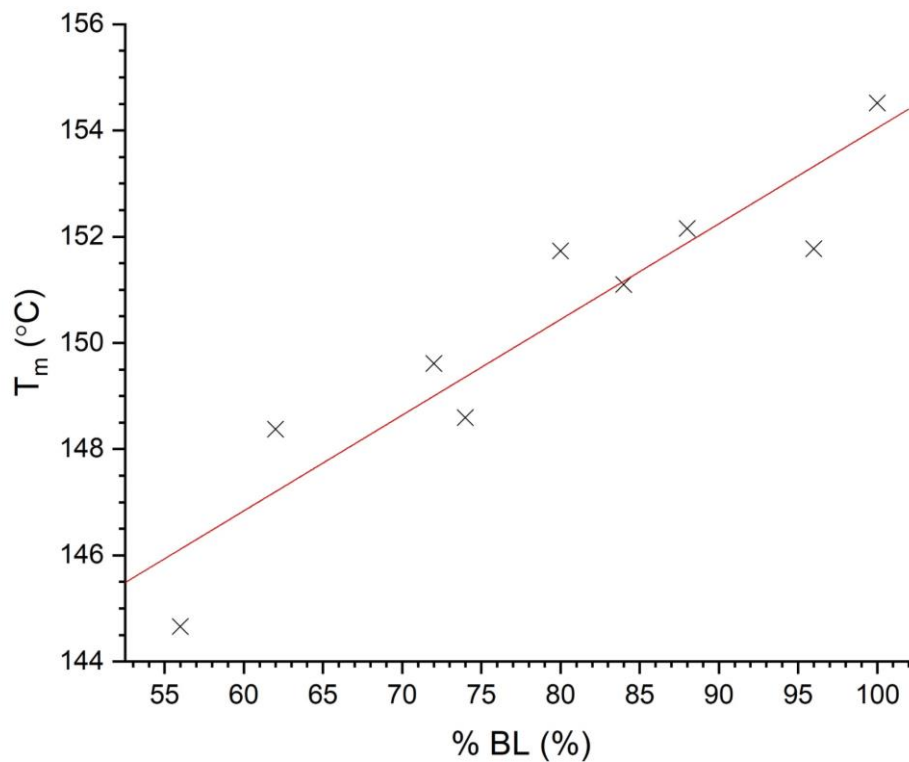
Figure 30: Plot of T_m vs. %BL. Line of best fit generated with equation:
$$T = 0.180\%BL + 136$$
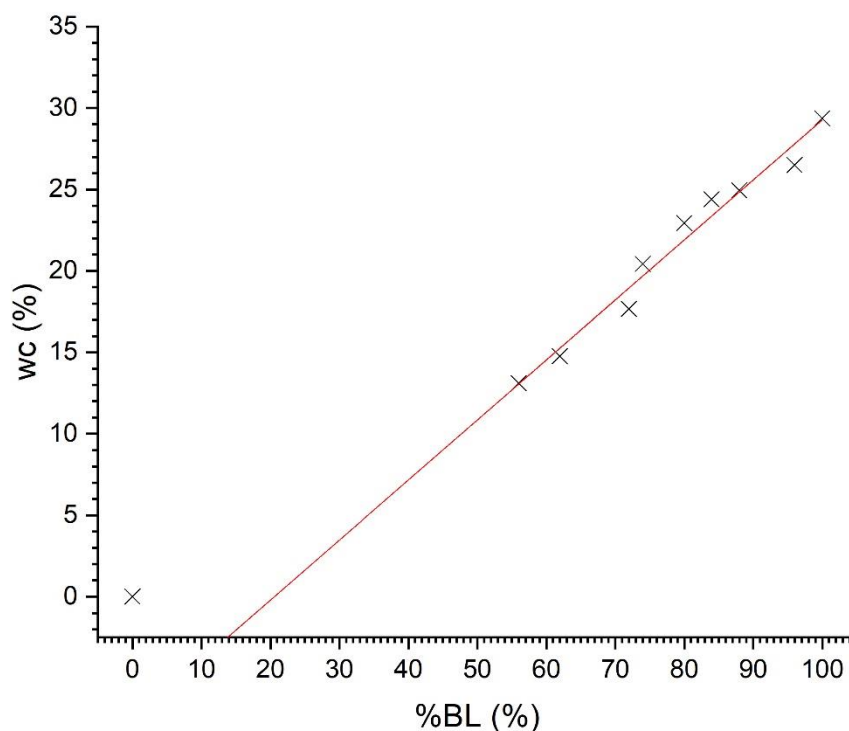
Figure 31: Plot of w_c vs. %BL in the polymer. Line of best fit generated with equation:
$$T = 0.369\%BL - 7.59$$

2.2.3 TGA

TGA was performed on 3 of the copolymers (**P1**, **P2**, and **P8**) and both the homopolymers (**P9** and **P10**) to determine if they thermally degrade above both the temperature of boiling water and their melting temperature. A graph was produced of mass loss as a percentage against temperature (**Figure 32**). This graph was directly used to determine T_o for each of the polymers (**Table 4**). The first derivative of the mass against temperature curve (**Figure 32**) was taken and plotted against temperature to produce a differential thermogravimetry (DTG) plot of mass change against temperature (**Figure 33**). The lowest peak on this graph is T_{max}, as tabulated in **Table 4**.
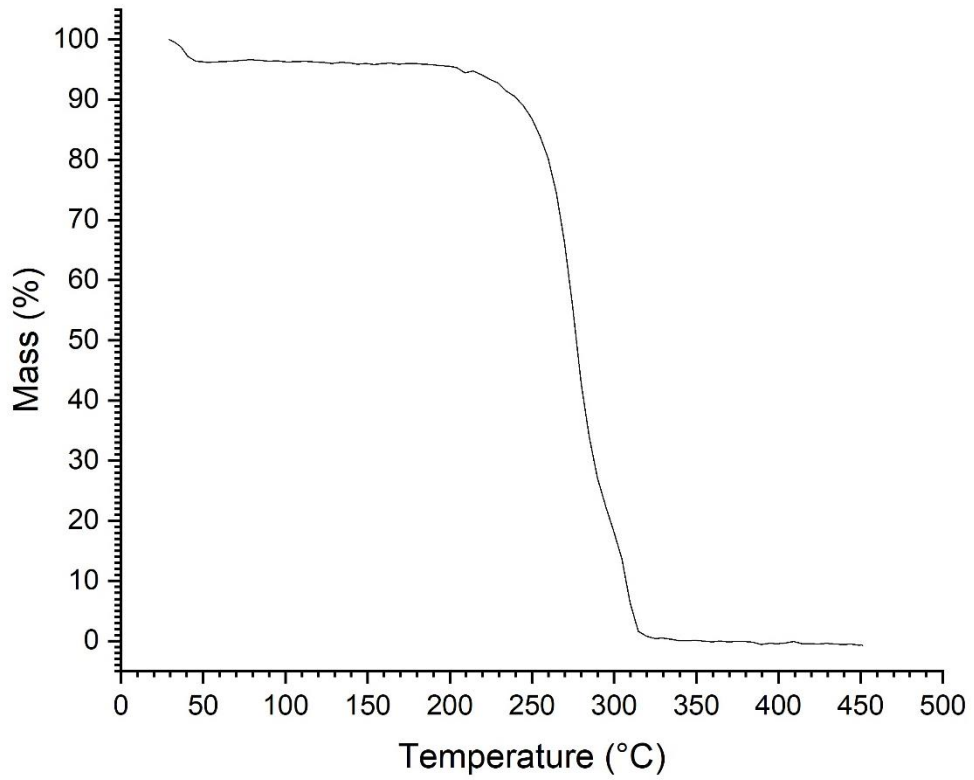
Figure 32: An example TGA curve for **P1**.
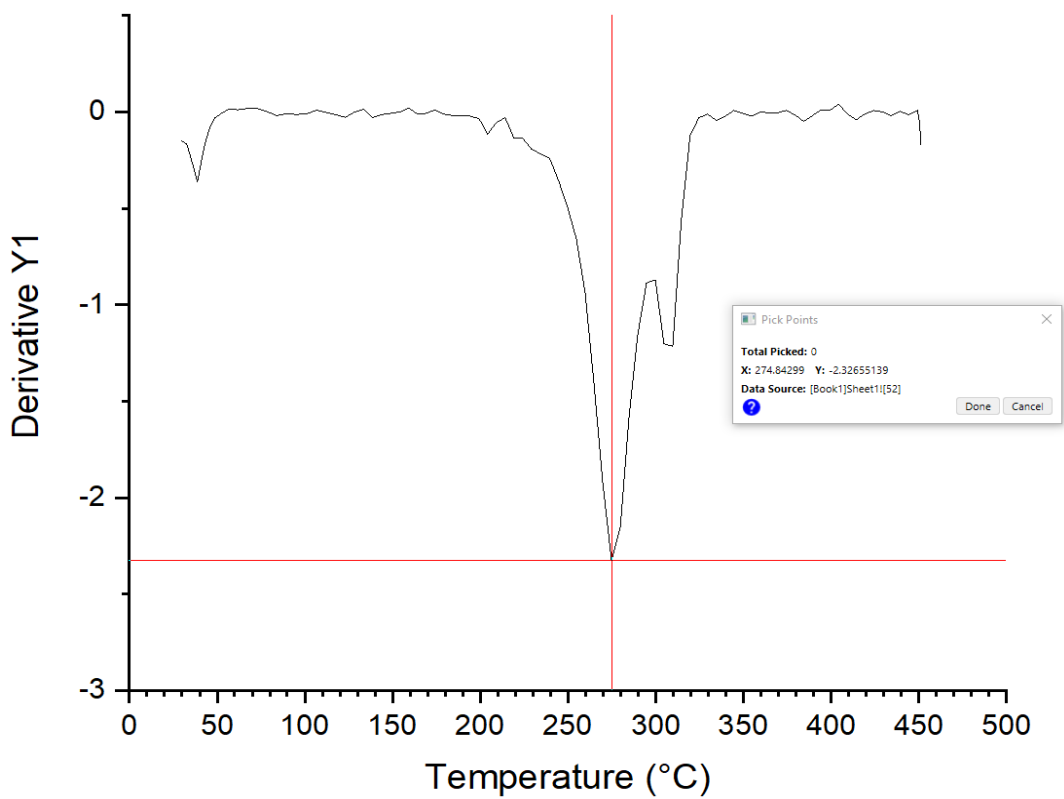
Figure 33: An example DTG curve for **P1**.

Table 4: The thermal data of the polymer samples as determined by TGA.

Polymer	Mass (mg)	T_O (°C)	T_{max} (°C)
P1	2.6960	219.24	274.84
P3	3.9000	209.16	272.25
P8	3.9180	211.70	269.65
P9	5.3110	226.87	267.13
P10	3.4020	224.34	292.27

The T_o and T_{max} temperatures were plotted against the %BL in the polymer (**Figure 34**). **P9** had the highest T_o value, with **P10** as a close second. Copolymers **P1**, **P3**, and **P8** were lower, with the lowest T_o value being 209.13 °C for **P3**. The polymers all have a T_o significantly higher than the boiling point of water which is essential for lining coffee cups as they will be expected to contain boiling water. In addition, the T_o is at least 59 °C higher than the T_m for each of the samples (excluding **P10** as this sample did not have a T_m), with the biggest difference being 74.58 °C for **P1**. This is seemingly a large range of temperature, however on an industrial scale this could be a narrow operating window between melting a significant quantity of the polymer and not causing degradation. The smallest difference between T_{max} and T_o was observed for sample **P9** at a value of 37.78 °C. The largest was for sample **P3** with a difference of 63.09 °C.
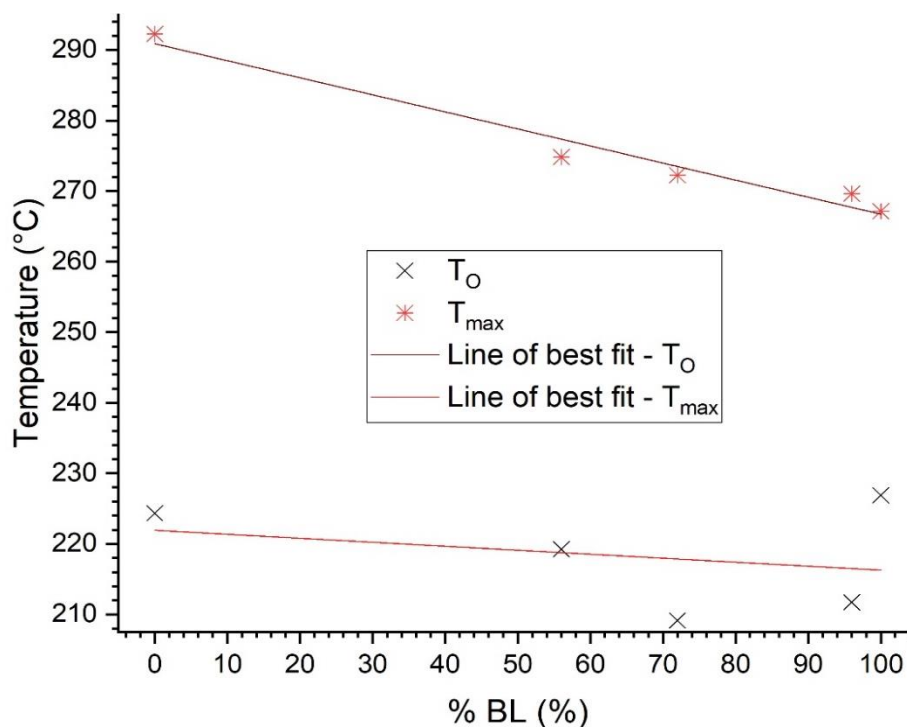
Figure 34: T_o and T_{max} vs. the %BL in the polymer.

2.2.4 GPC

All the crude polymer samples were prepared for GPC analysis. Before running the samples, the D_n/D_c values were determined for each of the compositions. These values were known for BL and LA; they were 0.0336 g/mL and 0.0237 g/mL respectively. **Equation 6** was used to determine the values for the various copolymer compositions (**Table 5**).

Equation 6: Calculation for determining the D_n/D_c values of the copolymer samples, where D_n/D_cBL and D_n/D_cLA are the D_n/D_c values for BL and LA respectively.

$$\frac{Dn}{Dc} = \frac{\%BL}{100} \times \frac{Dn}{Dc}BL + \frac{\%LA}{100} \times \frac{Dn}{Dc}LA$$

The theoretical number average molecular weight ($M_{n,\,theo}$) for each polymer was calculated using **Equation 7**, where the RMM of BL and LA were 86.09 g/mol and 144.13 g/mol respectively.

Equation 7: Equation used to calculate $M_{n, theo}$ of each of the copolymers, where M_rBL and M_rLA are the RMM values for BL and LA respectively.

$$M_{n,theo} = \left[M_r BL \times \left(800 \times \frac{\%BL}{100} \right) \right] + \left[M_r LA \times \left(800 \times \frac{\%LA}{100} \right) \right]$$

The chain length of each polymer was also calculated using **Equation 8**.

Equation 8: Equation used to calculate the average chain length of each of the polymers.

$$Chain\ length = \left[\frac{\frac{\%BL}{100} \times M_n}{M_r BL} \right] + \left[\frac{\frac{\%LA}{100} \times M_n}{M_r LA} \right]$$

Table 5: M_n and PDI values for the crude polymer samples, as determined by GPC performed in chloroform, with reference to polystyrene standards. Also, the calculated $M_{n, theo}$ and chain length values for each of the samples.

Polymer	D_n/D_c	$M_{n, theo}$ (kDa)	M_n (kDa)	PDI	Chain length
P1	0.0292	88.53	62.47	1.078	597
P2	0.0294	83.95	60.63	1.030	596
P3	0.0308	81.38	63.53	1.067	655
P4	0.0310	77.89	58.83	1.055	612
P5	0.0316	77.06	66.87	1.043	714
P6	0.0320	72.25	65.13	1.061	708
P7	0.0324	67.78	65.68	1.034	726
P8	0.0332	64.12	46.26	1.054	529
P9	0.0336	65.43	43.27	1.048	503
P10	0.0237	115.30	68.23	1.219	473

Table 5 shows the results from GPC analysis of the crude polymer samples. The measured M_n values were the same order of magnitude as the $M_{n, theo}$ values, which demonstrated good reaction control by the catalyst. The PDI values were all lower than 1.10 (except for **P10**) which indicated the polymer samples were highly uniform. This again showed good reaction control by the catalyst. Exception **P10** had a PDI value of 1.219, which demonstrated a moderate variety of M_n for the sample.

This again demonstrated a good degree of reaction control from the catalyst.

2.2.5 Discussion

The NMR data shows high levels of activity and control from the catalyst, which was judged by the polymer composition and monomer conversion. The composition of the copolymers reflects the monomer feed in the reaction. Also, the conversions of LA were all 100% and the lowest conversion observed for BL was 89%. The percentages of hetero-linkages were approximately 1.6 times the %LA in the copolymer which shows the monomer units were distributed to produce random copolymers. The alternatives to this would be block copolymers or alternating copolymers[55], where the percentage of hetero-linkages would be 0% and 100% respectively.

From the thermal data determined using DSC and TGA, it was shown that as the %BL increased, so did the T_m, ΔH_m, ΔH_c, and w_c. In contrast, with increasing %BL, the T_g and T_{max} both decreased. PHB (**P10**) was the most crystalline sample, so it follows that as the %BL increased, so did the w_c. PHB could be more crystalline than PLA due to higher symmetry in PHB which allows the chains to pack more efficiently.[55] More efficient packing could possibly lead to stronger intermolecular forces between the chains, as the dipole-dipole interactions between the carbonyl groups on neighbouring chains[55] could be more frequent.

Furthermore, it follows that the more crystalline the polymer, the more energy needed to melt or crystallise it. In crystalline phases, there is long range atomic order to the polymer chains, which leads to strong intermolecular forces between the polymer chains. The higher the w_c, the larger the crystalline phase is in the polymer sample, the more intermolecular forces there are that need to be broken in order for the crystalline phases of the polymer sample to melt. Hence, the T_m, ΔH_m and ΔH_c increasing with increasing %BL. PHB (**P10**) has a higher T_m than PLA (**P9**) which was amorphous so did not melt. Consequently, as %BL increased, so did the T_m. The reverse was true for T_g; as the %BL

increased, the T_g decreased. As a result, the gap between T_g and T_m increased as the %BL increased. This could be due to the increased w_c of the copolymer associated with increasing %BL. Pure PHB (**P10**) has lower T_g, and higher w_c and T_m than the amorphous PLA (**P9**) that was synthesised. As a result, the higher the %BL in the copolymer, the lower the T_g and the higher the w_c and T_m of the copolymer.

The T_o remained constant to within 15.2 °C. However, the T_{max} decreased with increasing %BL. This is due to PHB (**P9**) having a lower T_{max} than PLA (**P10**). As a result, as the %BL copolymer increases, the T_{max} decreases.

The GPC data showed all the polymers had M_n values to the same order of magnitude (10^4). Subsequently, the chain length of the polymers were the same order of magnitude (10^3). In addition, all PDI values were less than 1.100 (except **P10** which was 1.219). This again demonstrated high levels of activity and control from the catalyst.

2.3   FILMS

Only films made by solvent casting methods were analysed.

2.3.1 PXRD

PXRD was performed to produce graphs of 2ϴ vs counts (**Figure 35**), where the counts (black line) were how many X-rays are reflected and received by the detector (see section 1.5.4). In **Figure 35**, the blue line represented the background noise detected by the detector. The green line was the difference between the observed counts and the background. Finally, the red line was the difference added to the background to determine the calculated counts value.
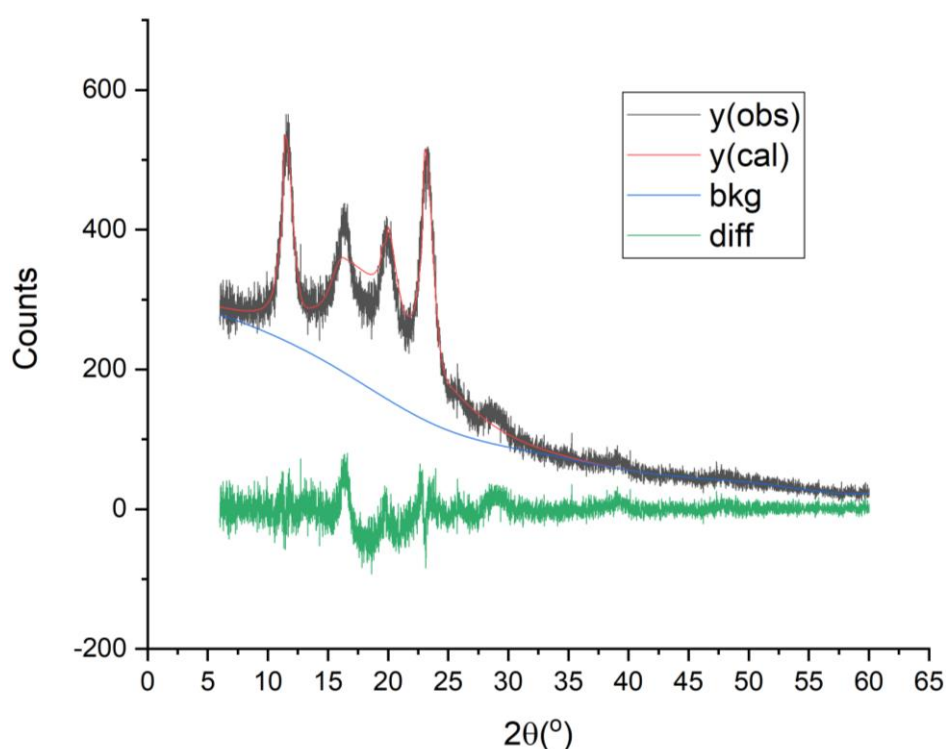
Figure 35: The PXRD spectra produced for sample **P9**.

The PXRD software could not be used to determine the w_c, so 2ϴ vs counts was plotted in Origin. Each of the crystalline peaks and the one amorphous peak were plotted as Gaussian peaks (**Figure 36**). The areas under these were used to calculate the crystallinities (**Table 6**).

Whilst this method of processing the PXRD data will not give accurate values for the w_c of the samples, using this consistently throughout this

project allows for trends to be established and an evaluation of relative crystallinity between the samples.

Equation 9: Equation used to calculate the w_c of the polymers.

$$w_c\ (\%) = \frac{Area\ of\ crystalline\ peaks}{Area\ of\ all\ peaks} \times 100$$
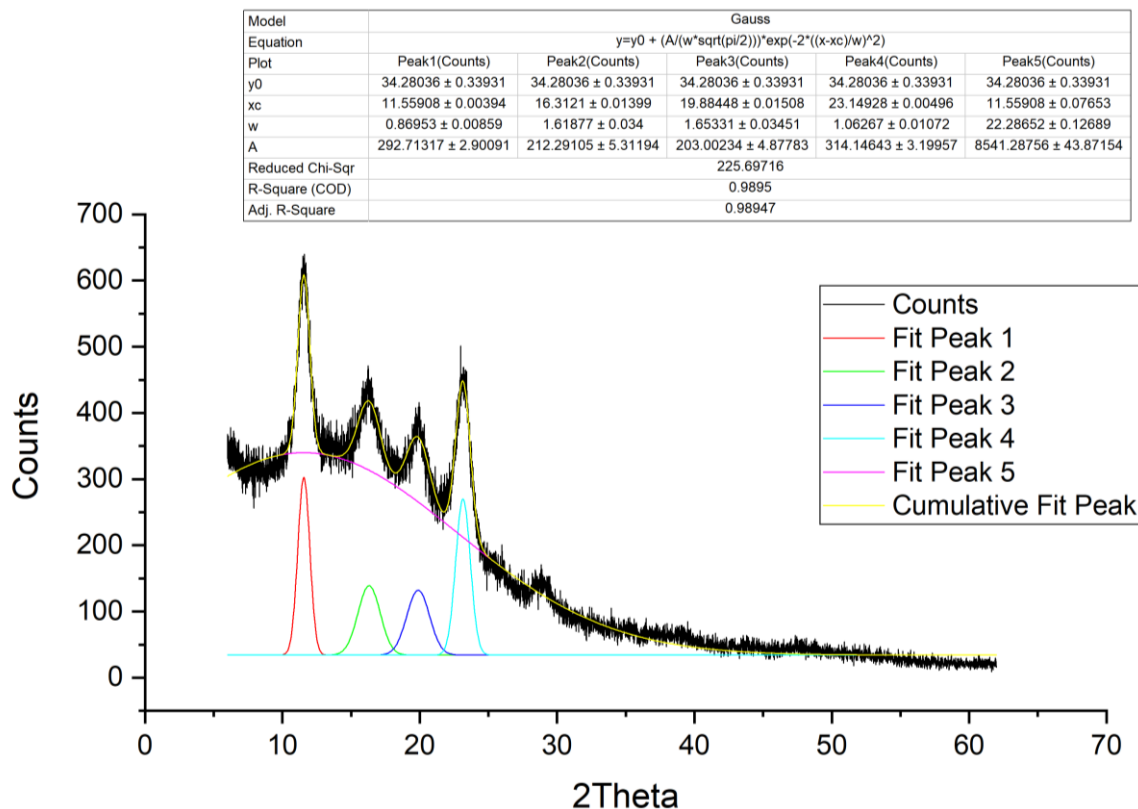
Figure 36: The PXRD data of sample **P8** after it had been processed in Origin.

Table 6: W_c of the polymer film samples as a percentage.

Polymer	W_c (%)	W_c from DSC [Table 3, p42](%)
P1	0.4	13
P2	7.0	15
P3	5.9	18
P4	11.7	20
P5	5.5	23
P6	10.3	24
P7	2.8	25
P8	12.9	27
P9	21.0	29
P10	0.0	0

In **Table 6**, the w_c data from DSC analysis was included for comparison. Both the w_c data from PXRD and from DSC analysis were graphed (**Figure 37**). The data produced from the DSC shows a much clearer trend than from the PXRD. Therefore, the data produced from DSC analysis appears more reliable, and the data from the PXRD less so. The lack of correlation in the PXRD data could be due to errors that arose from fitting Gaussian peaks to the curve during data processing. Using PXRD software that is specific for polymer analysis (not available at Lancaster University) may have led to more reliable results from the data processing.
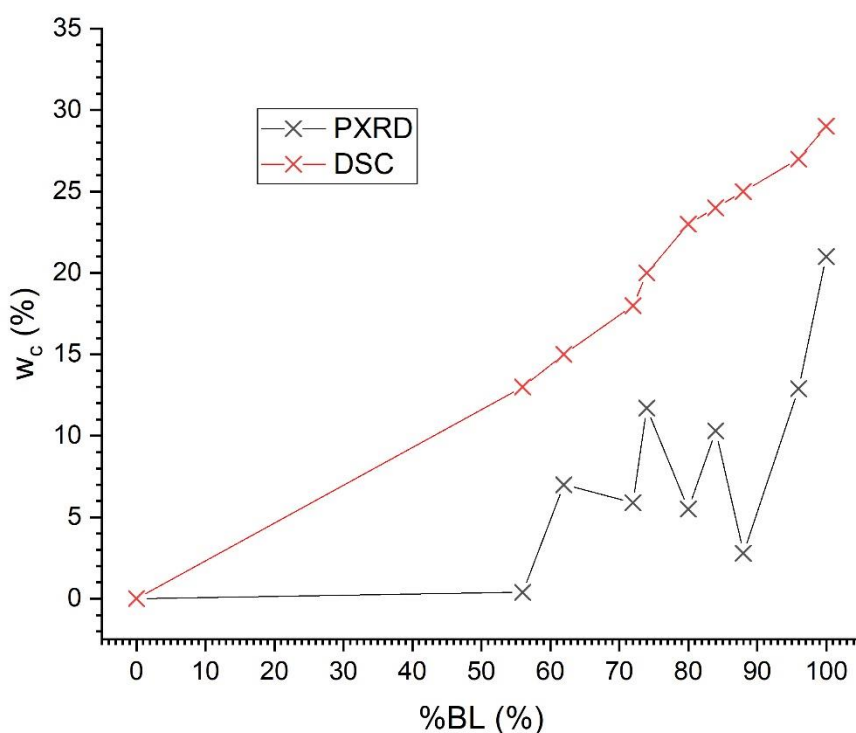
Figure 37: A graph of %BL vs the w_c as determined by DSC (red crosses and line) and PXRD (black crosses and line).

2.3.2 SEM

SEM was used to view the surface of the polymer films made from solvent casted samples **P5**-**P9**. Each of the polymer film samples were divided into three pieces, two of which were subjected to two tests, and the other was kept as a control. One piece was submerged in deionised

water (DI, test W2), and one piece was submerged in 95 °C DI (test HW2). All 3 pieces for each of the polymer films were compared using SEM. To compare the samples, the average number of holes/craters per 20 μm^2 were calculated for each sample, and the average diameter of the holes/craters were also determined (**Table 7**).

Table 7: A summary of the average number of holes/craters found in each polymer film sample, before water exposure (-), after water exposure (W2), and after hot water exposure (HW2). Also, an average diameter of the holes/craters found in each sample was determined.

Polymer	Treatment	Average No. Holes per 20 μm^2	No. of 20 μm^2 Squares Analysed	Average Diameter of Holes (μm)
P9	-	0.000	277	-
	W2	0.000	184	-
	HW2	0.007	284	0.264
P8	-	0.000	160	-
	W2	0.002	248	0.147
	HW2	0.001	145	0.148
P7	-	0.000	164	-
	W2	0.002	132	0.147
	HW2	0.002	102	0.072
P6	-	0.000	83	-
	W2	0.008	300	0.137
	HW2	0.023	136	0.124
P5	-	0.000	109	-
	W2	0.003	108	0.275
	HW2	0.004	232	0.162

No holes/craters were observed in any of the control samples. After exposure to DI water, all the samples exhibited holes/craters. The only exception was **P9**, which did not have any holes/craters present after exposure to room temperature DI water. It is possible that holes/craters were present in the sample but were not observed in the random sample chosen for analysis. It is notable that the surface of the films were changed by water exposure. The range of average hole/crater diameters was 0.072-0.275 μm, which is considerably larger than a molecule of water which is approximately 2.8 Å in diameter.[77] However, due to the surface tension of water and the hydrophobic nature of the polymers, it was possible that water may not pass through these potential holes.

In **Figure 38**, it can be observed that most of the polymer films appear smooth, and lack features. So, after water exposure the main difference between the films subjected to the W2 and HW2 tests and the control, was the formation of holes/craters. Otherwise, the samples appear very similar between the controls (a) and the W2 (b) and HW2 (c) samples for each of the polymers tested. The other polymer samples (**P1**-**P4**, and **P10**) were also tested. However, due to financial reasons, not all the samples could be analysed by SEM. Therefore, analysis moved on to practical water permeability tests. **P10** was going to be analysed so that both the homopolymers could be used as comparison, however the sample repeatedly shrivelled in the HW2 test and so was not able to be analysed by SEM.

EDX was also used to analyse what elements were present in the films. Varieties of elements were found that were deemed to be from contamination due to working in a communal laboratory. Two elements of interest were found. Chlorine was found numerous times which could be present due to dissolving the polymer in chloroform to cast it as a film. This could suggest the presence of residual chloroform. Alternatively, chlorine could be present from contamination as it is part of common reagents such as brine. The second element of interest was yttrium. This was found 15 out of 74 occasions, thus yttrium was found in the films 20% of the time. The highest amount found was 4.5 wt%, with the average amount across the 15 times yttrium was found being 1.4 wt%. This suggests that not all the catalyst was removed in the purification process. Also, based on the polymerisation parameters, it seems the catalyst has accumulated in areas in the polymer film. In the polymerisation reactions, there was 16 mmol of monomer and 0.02 mmol of catalyst used. The weight percentage of yttrium when using 16 mmol of LA or BL is 0.1% and 0.01% respectively in each homopolymer synthesis, and somewhere in between for the copolymerisations. This could be detrimental to these polymers being used to line coffee cups as ideally, yttrium should not be in the final product as it could be harmful.
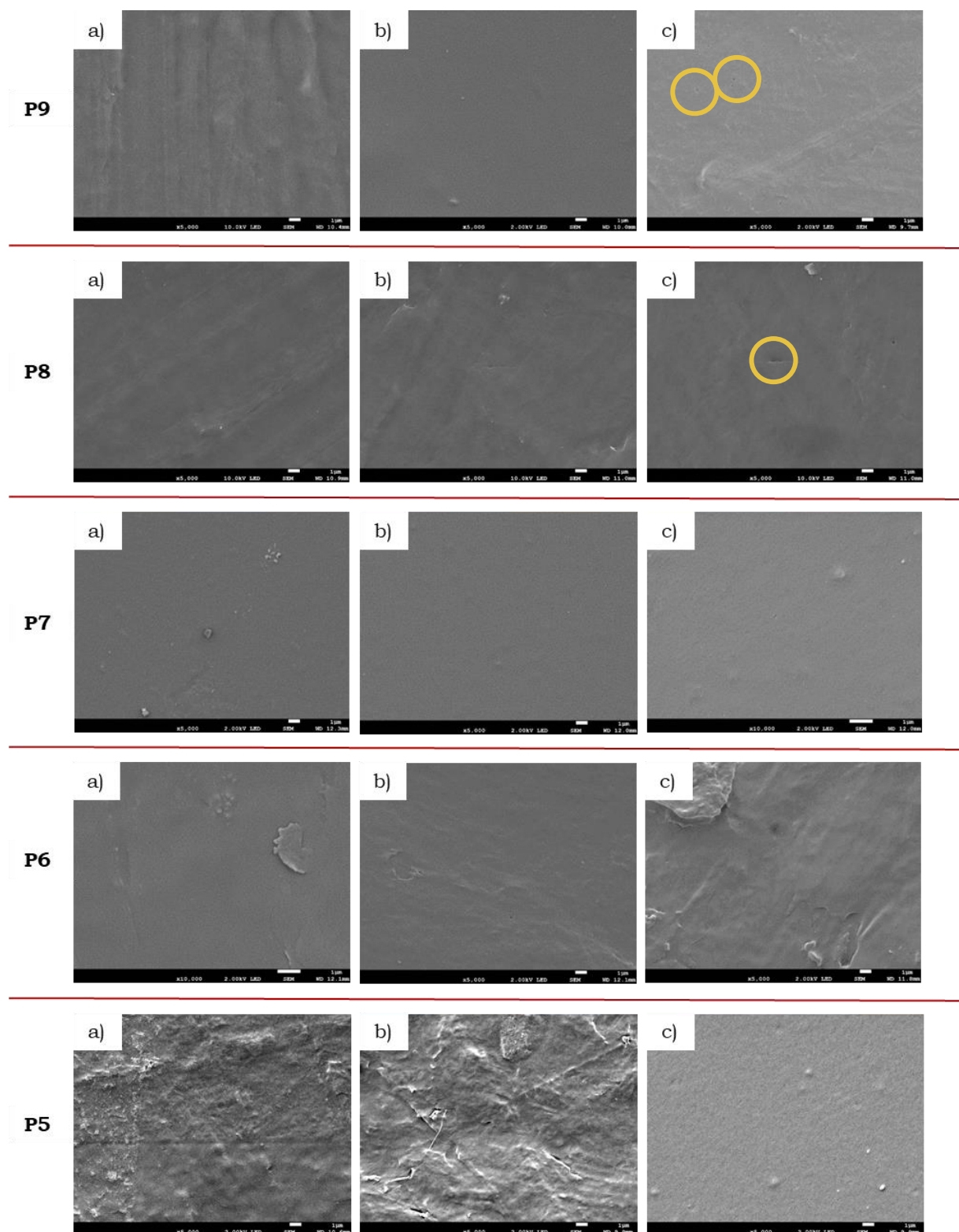
Figure 38: A sample of the SEM images acquired for each of the samples in **Table 7**. Each row is a set of images from each polymer sample. A) An image from the control sample. B) An image from a sample subjected W2. C) An image from the sample subjected to HW2. All images were taken at a magnification of x5000, except **P6**a which was taken at x10000. For all images the probe was set to 2.0 kV, except **P9**a, and all **P8** samples where the probe was set to 10.0 kV. All scales bars are 1 μm in length. A few of holes have been highlighted with a yellow circle.

2.3.3 Water Permeability Tests

2.3.3.1 Cobalt Chloride Paper

The films needed to be tested for their water permeability within the context of being used for a single-use beverage cup. Therefore, the films needed to be tested when they are bound to cup paper, in a way where the films performance is the only variable. As PE is currently melted onto cup paper, the polymer films were melted onto uncoated cup paper in an oven at 160 °C for 30 minutes. The film coated paper was then allowed to cool. A piece of glass was then weighted onto the top of the film so that room temperature DI water could be poured into this glass vessel, however it could not spread onto areas of uncoated paper as the glass prevented this. Underneath the cup paper, a piece of anhydrous cobalt chloride paper was placed. This paper was blue, however if any water came through the film and card, it turned pink (**Figure 39**). After 10 minutes, the set-up was deconstructed, and the cobalt chloride paper was analysed for water intrusion.
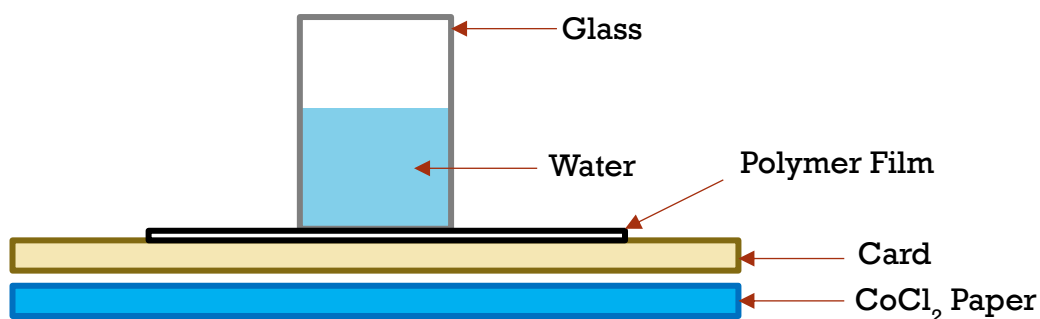
Figure 39: A diagram of the water permeability testing set-up using cobalt chloride paper.

As can be observed in **Figure 40**, the paper indicated when water passed through by changing colour from blue to pink as observed in the yellow circle. However, the paper would also discolour around the edges due to atmospheric moisture. This made this method unsuitable for longer term testing.
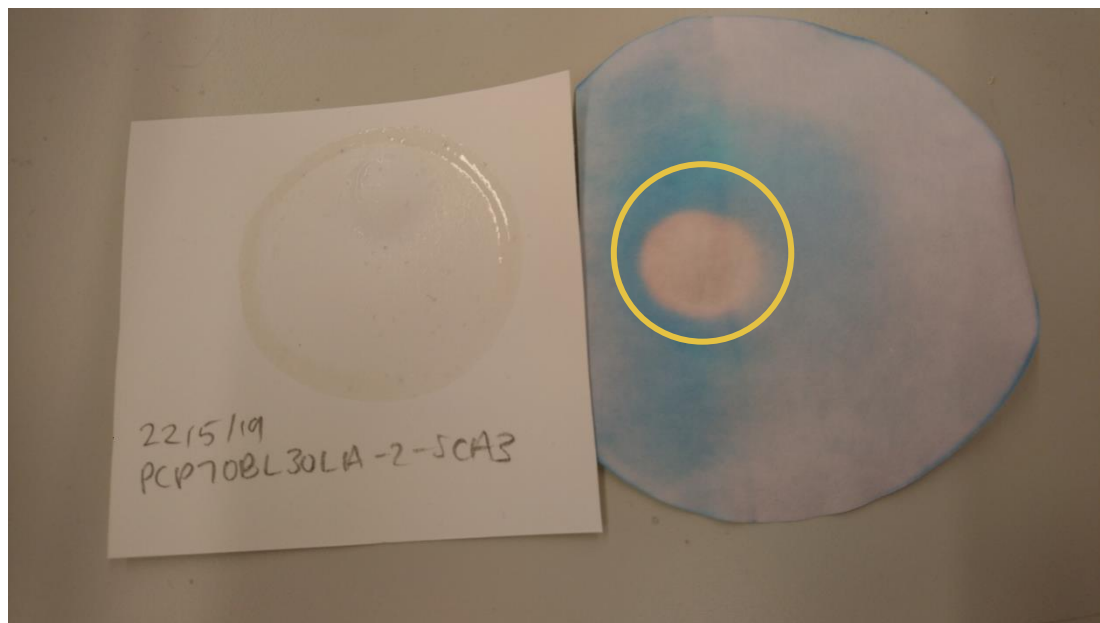
Figure 40: Outcome of the water permeability test using cobalt chloride paper as an indicator with **P3**. The blue area is where the $CoCl_2$ had remained anhydrous. The pink area around the edge is where atmospheric water had hydrated the $CoCl_2$. Inside the yellow circle is where the water was purposefully held on top of the polymer film. The colour of the paper has changed from blue to pink, indicating that water had permeated the film and cup paper.

Some copolymers were tested (**Table 8**). **P2** and **P3** both allowed water to pass through which was clearly indicated by the paper changing colour from blue to pink. **P8**, which was one of the best performing copolymers by SEM analysis, was then tested. This did not allow to water to pass through, as demonstrated by the cobalt chloride paper remaining blue. **P3** also did not allow water to pass through when it had been made using 3 times the amount of copolymer (**P3 – x3** in **Table 8**). This is probably due to any craters forming in the surface of the film being unable to turn into holes. Also, as the test could only be performed for 10 minutes, with more time the water may still have passed through.

Table 8: Water permeability test results after 10 minutes of water exposure.

Polymer	Cobalt Chloride Paper Colour	Water permeable?
P2	Pink	✓
P3	Pink	✓
P8	Blue	X
P3- x3	Blue	X

2.3.3.2 Fluorescein Dye

As the cobalt chloride paper only allowed for a 10 minute long test, another test was needed to determine the water permeability of the film when it was melted on paper. Typically, a consumer would have a hot drink for longer than 10 minutes so a test was required that could be run for a longer period. Fluorescein dye is an inert, non-hazardous dye that is fully soluble in water. This dye was made at a concentration of 0.1 mg/mL in water. This solution was added to the film that was melted onto uncoated cup paper with some filter paper underneath (**Figure 41**). This was left for 24 hours and analysed to determine if any dye had passed through, which would indicate that water would have also passed through.
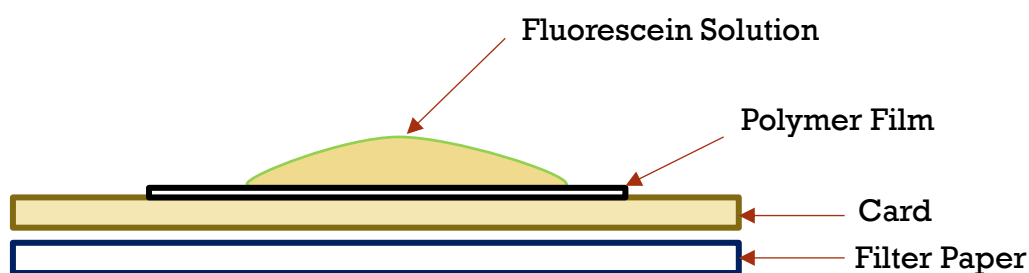
Figure 41: A diagram of the water permeability test set-up using fluorescein dye.

A control was performed by applying the dye solution to the uncoated paper with no film. This test failed; the dye was visible on the underside of the card (**Figure 42**) both with the naked eye (b) and under UV light (c). Due to its intense fluorescent properties, even if a small amount of the dye passed through the film and paper, under UV light the dye would be visible. It is important to note that this experiment technically tests the permeability of the dye. However, the liquid water droplets are bigger than the molecular scale. Consequently, it reasonable to assume that if the dye passed through, the water had as well. This control verified this test as a way of indicating water permeability of the film once it had been melted on the card.
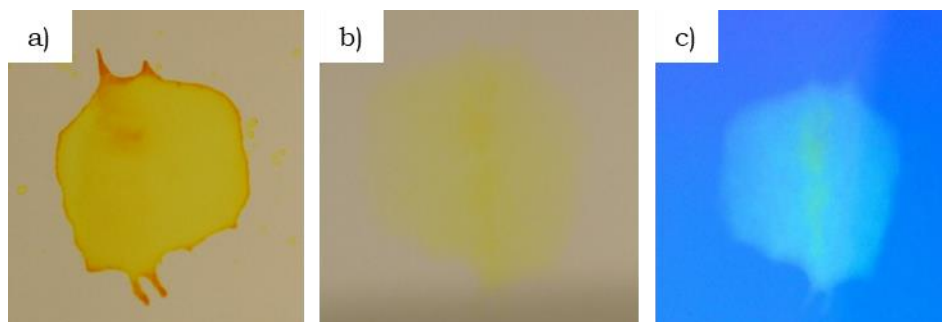
Figure 42: The results of the control for the water permeability test using fluorescein solution. A) The paper where the dye solution had been applied. B) The underside of the paper that, where it can be observed that the dye solution had permeated the film and cup paper. C) The underside of the paper as observed under UV light, where it can be observed that the dye solution has permeated the film and cup paper.

This was repeated with a selection of polymer films that had been melted onto the uncoated cup paper. The results are summarised in **Table 9**. The top row is the results from the control test, as described in **Figure 42**. **P9** did not show any dye colour on the underside of the card; however, the dye was visible under UV light. Therefore, water had passed through during the 24 hours. Similar was true for **P1** and **P3** (**Figure 43**), although this time the yellow colour of the dye had come through the card and could be observed with the naked eye. However, it is not visible on photograph b in **Figure 43**. Although, the UV fluorescence of the dye is clearly observable in photograph c. For the melted polymer films made from samples **P5**-**P8, P1**, and **P10**, no dye was observed on the underside of the card under natural or UV light as observed in **Figure 44**.

Table 9: Water permeability test results from 24 hours water exposure.

Polymer	Polymer Composition BL/LA	Dye Visible?	Dye UV Visible?	Water permeable?
No Film	-	✓	✓	✓
P1	56/44	✓	✓	✓
P2	62/38	X	X	X
P3	72/28	✓	✓	✓
P3- x3	72/28	X	X	X
P4	74/26	X	X	X
P5	80/20	X	X	X
P6	84/16	X	X	X
P7	88/12	X	X	X
P8	96/4	X	X	X
P9	100/0	X	✓	✓
P10	0/100	X	X	X
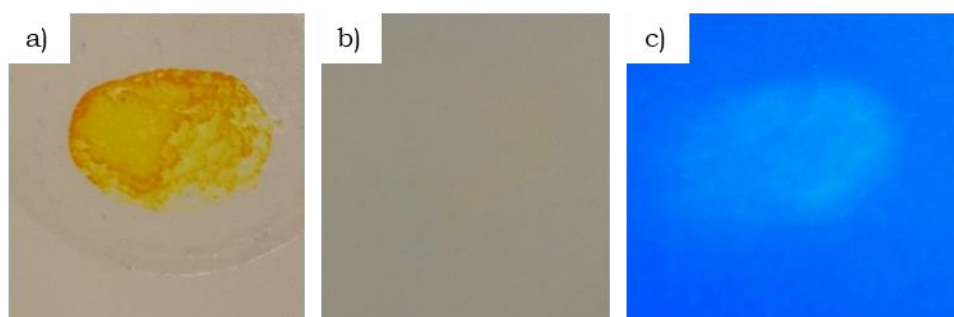
Figure 44: The results from the water permeability test on **P3** that had been melted on paper. A) The film where the dye solution had been applied. B) The underside of the paper, where there was no dye visible. C) The underside of the paper as observed under UV light, where it can be observed the dye solution had permeated the film and cup paper.
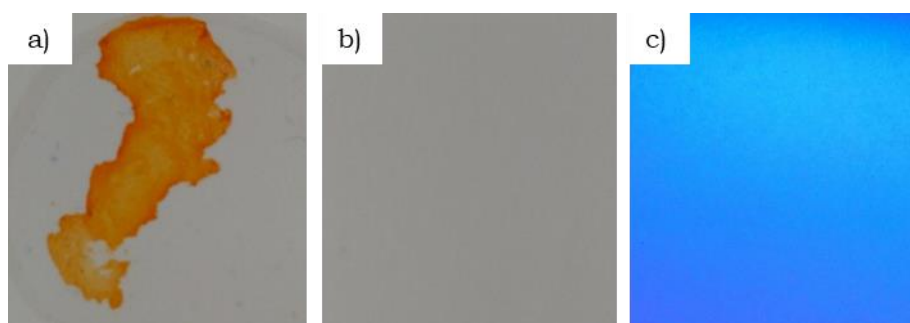

Figure 43: The results from the water permeability test on **P8** that had been melted on paper. A) The film where the dye solution had been applied. B) The underside of the paper where there was no dye visible. C) The underside of the paper as observed under UV light, where it can be observed the dye solution had not permeated the film and cup paper.

2.3.3.3 Discussion

In general, for copolymers **P1**-**P8**, as the %BL increased, the polymer samples become impermeable to water. This could be due to the increase in crystallinity. Amorphous polymers are more likely to allow water to pass through if they are above their T_g as the chains are mobile. A crystalline polymer or an amorphous polymer below its T_g is less likely to be water permeable as the water cannot penetrate the amorphous phases as easily as the chains are immobile. As the crystallinity increases, the diffusing molecules (water or the fluorescein dye) need to take a more tortuous path, around the impermeable crystalline phases, to pass through amorphous phases of the film and the cup paper. Also, as the crystallinity increases, the size of the crystallites increases, which restricts the mobility of the crosslinking chains.[52] This reasoning could also account for why **P9** is water permeable and **P10** is not. **P9** and **P10** had a T_g of 1.15 °C and 41.32 °C respectively. The water permeability tests were performed at room temperature. This is above the T_g of **P10** but below the T_g of **P9**. Therefore, the chains amorphous phases of **P10** would be mobile, so more likely to pass through. The opposite would have been true for **P9**. Based on this idea, if this water was at 100 °C, all the polymer films would be more likely to be water permeable as all of the polymers would be above their T_g. It is plausible that a mixture of the w_c and T_g contributed to the water permeability of these films. It is worth noting that the T_g of LDPE currently used in coffee cups is – 125 °C.[17] To evaluate the impact of the temperature being above or below the T_g of the copolymers, this water permeability test should be repeated in a temperature controlled environment at a temperature below and above the T_g of each sample.

2.3.4 Seam Test

During manufacture, the lined cup card is folded round to form a cup shape, and the PE is melted using ultrasonic heating between the overlapping cards to form a seam. Pressure is also used to hold the seam in place whilst the polymer melted. It is ideal for the replacement

polymer lining to serve this function as well so one of the samples was tested. The film melted successfully between the overlapping pieces of uncoated cup paper (**Figure 45**, a) in an oven at 160 °C. It could be held on one side without the other piece of cup paper coming away. However, when a small amount of pressure was applied to pull both pieces away from each other in a linear fashion, the pieces came apart (**Figure 45**, b and c). However, this test was not an accurate reproduction of the industrial manufacture of these seams as there was no pressure applied to the seam during melting. Also, the polymer was melted in an oven, which differs from the industrial method which heats the polymer ultrasonically. Therefore, it is still plausible that the polymer samples made could form a robust enough seal along the seam of cups.
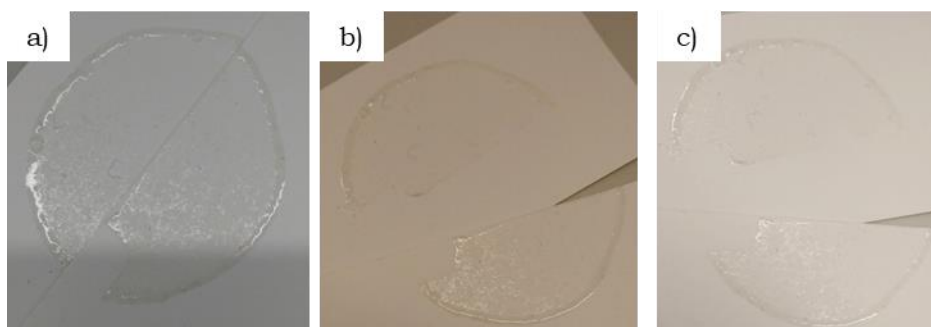
Figure 45: Seam test performed with a film made from **P4** that had been melted between overlapped paper. A) The film post melting. B and C) The film post seam test.

2.3.5 PE Coated Paper Comparison

The specification of the PE paper currently used by the Printed Cup Company was provided. The paper is coated in PE 15 g/m², which leads to a thickness of 10 μm of PE. When **P8** was casted and melted onto uncoated cup paper, 100 mg of polymer was used to produce a film that was 5.2 cm in diameter. Based on this, to produce a film that would be the same grammage (g/m²) as the PE card, 33 mg of polymer should be used to produce the same size film. This produced a fully formed, circular film. However, when it was melted to the cup paper (**Figure 46**), large holes appeared. The film may have shrunk during the melting process. From this test, it does not seem possible to produce a film using

P8 that is the same grammage metre as the current PE lining on uncoated cup paper that is fit for purpose.
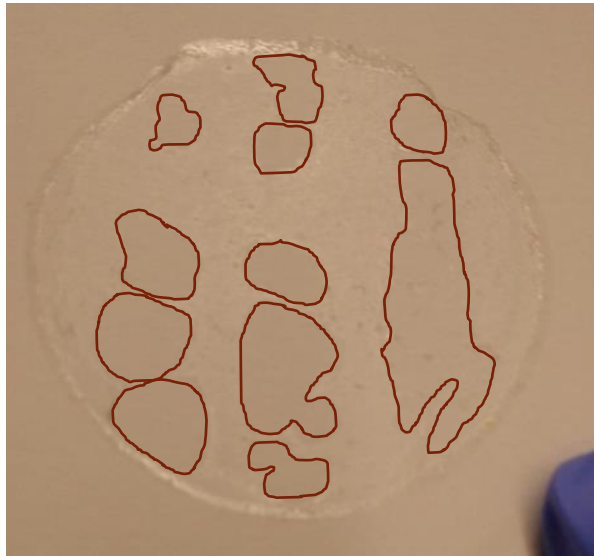
Figure 46: Film made using **P8** for melting onto paper. The burgundy shapes indicate a boundary between where the polymer film had melted onto the paper and where it had not. Inside the shapes was bare paper. Outside the shapes was where the film successfully melted onto the paper.

3   CONCLUSION

PE serves well as a lining for a paper cup to make them heatproof and leak-proof. However, it is not without its drawbacks. It is non-renewable and does not biodegrade. It also prevents the paper from biodegrading. With these points in mind, it is important to find a replacement for PE.

In this project, PLA and PHB copolymers have been investigated for their suitability to replace PE. To do so, the new polymer needs to be resilient to 100 °C water. It also needs to be chemically resistant to coffee and other foods or drinks that may be consumed from the cup. The replacement polymer also needs to form the seal on the seam of the cups, as PE currently does. In addition, the polymer should make the cups either easier to recycle or be biodegradable.

All the polymers tested had a melting temperature and thermal degradation temperature that was significantly higher than the boiling point of water, so all the polymers were subjected to further testing. The polymer films also showed that water and hot water changed their film texture when viewed by SEM. However, practical testing after melting the films onto uncoated cup paper showed that polymers **P5**-**P8**, **P1**, and **P10** do not allow room temperature DI to pass through in 24 hours. This is possibly due to a combination of the w_c of the sample and whether the test was performed above or below the T_g of the polymer. This shows potential for these polymers to be resilient to 100 °C water. Further testing (discussed in section 4) would be necessary to determine the polymers resistance to substances other than room temperature DI.

One polymer was used to determine whether the film could be used to form a seam. This polymer failed; however, there was only one test performed with one polymer film so further repetitions and an optimisation of the testing method to better reflect industrial methods would be necessary to draw well rounded conclusions from this.

Additionally, it was determined that the polymer films were being made at 3 times the grammage that the PE is currently coated onto paper at.

As a result, a polymer film was made in the same area but with a third of the amount of polymer to replicate the grammage used for PE coating on paper. When melted onto paper, this led to holes forming in the film. This was possibly due to the polymer contracting. It is viable for the replacement polymer to be thicker than the PE coating currently used (to an extent). However, there is extra costs associated with using more polymer per square metre to form the coating. This could make the new coating financially unavailable to companies.

EDX analysis showed that yttrium could be present in the final polymer film at as much as 4.5 wt% with a 20% chance of yttrium being present. In addition, the amount of yttrium in the polymerisation reactions was between 0.01-0.1 wt% so it appears that the yttrium accumulates in areas in the polymer film. This means that if these polymers were to be used in a product, a more effective or additional purification step in the synthesis of the polymers would be required to remove all the yttrium.

Spin coating of the polymers was attempted throughout this project; however, a technique was not perfected for these polymers within the time frame that reliably produced films of a good enough quality for further testing and analysis. In addition, the films can only be coated onto glass using this method, which limited the tests that could be performed.

Overall, all the polymers have melting points and thermal degradation temperatures significantly higher than the boiling point of water. After water permeability tests, it was determined that **P5**-**P8** are the most suitable samples to be subjected to further testing.

4   FUTURE WORK

The water permeability test using fluorescein dye should be repeated above and below the T_g of the all the polymer samples to assess whether the T_g contributes to the water permeability for these aliphatic polyesters. The polymer samples that show water resistance above their T_g should be subjected to a similar test using 100 °C water. Also, testing for resilience to hot, caffeinated water would be necessary and possibly directly testing using coffee if any polymers were still showing good resistance.

Further seam tests should also be conducted to establish whether the films could seal the seams of the cups. If not, maybe an additive could improve the polymers ability to do this. Furthermore, the thickness of the polymer film needs to be further investigated to determine the minimum amount of polymer that can be used to create sufficient water permeability and reliability when melting onto the uncoated cup paper.

The biodegradability and recyclability of the films were not tested. The biodegradability could be tested by burying the films in fertile soil, like Altaee *et al.*[44] For recyclability, a company that currently recycles cups could be contacted about the possibility of them testing the new films for their recyclability through their current methods. Another important consideration is whether the film affects the flavours of the beverages the cups contain. However, this consideration is important at a later stage in testing.

5   EXPERIMENTAL

All chemicals were purchased from Sigma Aldrich (Gillingham, UK), Fischer (Loughborough, UK) and Alfa Aesar (Heysham, UK), unless otherwise stated. BL was dried over calcium hydride and distilled before reacting. LA was dried by sublimation before use in reactions.
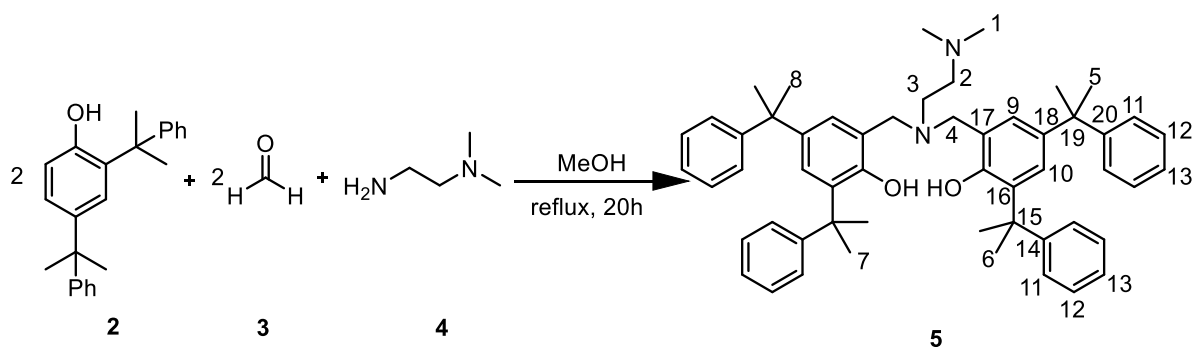
All NMR data were recorded on a Bruker Avance III 400 MHz NMR spectrometer (Bruker UK Ltd., Coventry, UK) at 298K. All NMR spectra were processed using MestreNova software.

All spectra and raw data are shown in the appendix.

5.1   SYNTHESIS AND CHARACTERISATION

5.1.1 Catalyst

5.1.1.1 Ligand

Figure 47: Reaction scheme for synthesis of the ligand.

This procedure was performed similar to Zhu *et al.*[72] Bis(α, α – dimethylbenzyl)phenol (**2**, 5 g, 15 mmol) was added to methanol (10 mL) and stirred until it was dissolved. Formaldehyde (**3**, 37% by weight in H_2O, 1.12 mL, 15 mmol) and *N,N*-dimethylethylenediamine (**4**, 0.819 mL, 7.5 mmol) was then added. The reaction mixture was heated at reflux for 20 hours. The reaction mixture was removed from the heat and allowed to cool for 1 hour. The white solid was then collected by vacuum filtration. The solid was washed with ice-cold methanol. The

sample was dried under vacuum at 60 °C. The yield was 4.50 g (**5**, 80.0%,).

¹H NMR (400 MHz, CDCl₃) δ 9.49 (s, 2H, OH), 7.27 (m, 8H, H_{11}), 7.20 (m, 12H, $H_{12/13}$), 7.09 (dt, J = 9, 3 Hz, 2H, H_{10}), 6.73 (d, J = 3 Hz, 2H, H_9), 3.39 (s, 4H, H_4), 2.31 (t, J = 6 Hz, 2H, H_3), 2.12 (t, J = 6 Hz, 2H, H_2), 1.69 (s, 12H, $H_{5/6/7/8}$), 1.67 (s, 6H, NMe_2), 1.65 (s, 12H, $H_{5/6/7/8}$).

¹³C NMR (101 MHz, CDCl₃) δ 152.9 (C-O), 151.5 ($C_{16/17}$), 151.5 ($C_{16/17}$), 139.4($C_{14/20}$), 135.8 ($C_{14/20}$), 127.8 (C_{11}), 127.4 ($C_{12/13}$), 126.9 (C_9), 126.8 (C_{11}), 125.9 ($C_{12/13}$), 125.3 ($C_{12/13}$), 125.2 ($C_{12/13}$), 124.5 (C_{10}), 121.9 (C_{18}), 56.5 (C_4), 56.0 (C_2), 48.6 (C_3), 44.2 ($C_{5/6/7/8}$), 42.4 ($C_{15/19}$), 42.0 ($C_{15/19}$), 31.1 ($C_{5/6/7/8}$), 29.3 ($C_{5/6/7/8}$).

5.1.1.2 Catalyst Synthesis
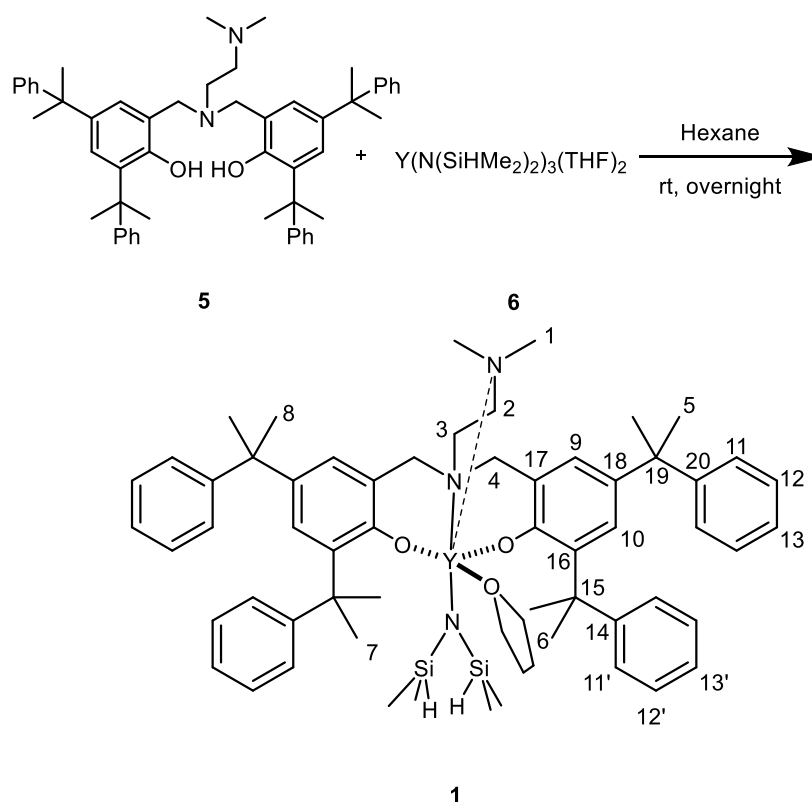
**Figure 48**: Reaction scheme for the formation of the catalyst.

This procedure was adapted from Bouyahyi *et al.*[56] 2,2'-[[[2-(dimethylamino)ethyl]imino]bis(methylene)]bis[4,6-bis(1-methyl-1-phenylethyl)-phenol (**5**, 0.630 g, 1 mmol) and Y(N(SiHMe₂)₂)₃(THF)₂ (**6**, 0.750 g, 1 mmol), provided by Dr. Rachel Platel, was added to dry

hexane (8 mL) under an atmosphere of nitrogen. The reaction mixture was stirred overnight. The solvent was removed under vacuum to obtain a crude white solid. Hexane was added (5 mL) and a white precipitate formed. The sample was left in the freezer overnight. The colourless solid (**1**, 0.686 g, 64.4%) was collected by vacuum filtration.

¹H NMR (400 MHz, C₆D₆) δ 7.41 (d, J = 2.5 Hz, 2H, H_{10}), 7.35 – 7.26 (m, 8H, $H_{11}, H_{11'}$), 7.13 – 7.03 (m, 8H, $H_{12}, H_{12'}$), 6.98 (tt, J = 8, 4 Hz, 2H, $H_{13/13'}$), 6.86 (t, J = 7 Hz, 2H, $H_{13/13'}$), 6.73 (d, J = 2.5 Hz, 2H, H_9), 4.72 (m, 2H, $(SiH)_2$), 3.33 (d, J = 12.5 Hz, 2H, $C_4H_AH_B$), 2.97 (s, 4H, THF), 2.34 (d, J = 12.5 Hz, 2H, $C_4H_AH_B$), 2.01 (s, 6H, H_6, H_7), 1.77 (s, 6H, H_6, H_7), 1.65 (s, 6H, $H_{5/8}$), 1.64 (s, 6H, $H_{5/8}$), 1.62 (s, 6H, NMe_2), 1.00 (s, 4H, THF), 0.35 (s, 12H, $(SiMe_2)_2$).

¹³C NMR (101 MHz, C₆D₆) δ 161.5 (C-O), 152.7 ($C_{16/17}$), 152.0 ($C_{16/17}$), 135.7 ($C_{14/20}$), 135.5 ($C_{14/20}$), 128.3 (C_9), 127.9 ($C_{12/12'}$), 127.7 ($C_{12/12'}$), 127.6 (C_{18}), 127.4 (C_{18}), 126.9 ($C_{11/11'}$), 126.5 ($C_{11/11'}$), 126.4 (C_{10}), 125.4 ($C_{13/13'}$), 124.7 ($C_{13/13'}$), 124.4 ($C_{13/13'}$), 70.6 (THF), 64.6 (C_4), 45.0 ($C_{5/8}$), 42.7 ($C_{15/19}$), 42.3 ($C_{15/19}$), 31.6 ($C_{2/3}$), 31.3 ($C_{5/8}$), 28.7 ($C_{6'/7'}$), 22.7 (THF), 4.6 (($SiMe_2)_2$).

5.1.2 Polymerisations
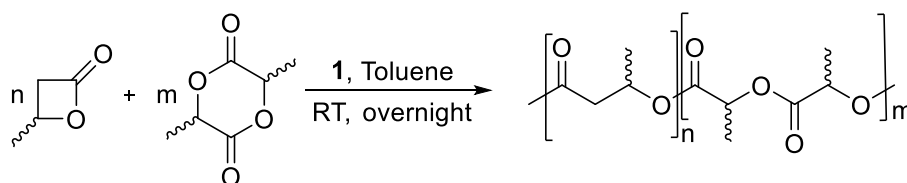
Figure 49: General reaction scheme for polymerisations.

BL and LA (amounts in **Table 10**) were dissolved in toluene (30 mL). Separately, **1** (0.02 mmol, 0.022 g) was dissolved in toluene (2 mL) before being added to the reaction mixture. The reaction was stirred overnight. It was then quenched with hexane (approx. 40 mL). The excess hexane was decanted, and the remaining solvent was left to evaporate overnight to leave the crude polymer. The polymer was dissolved in the minimum amount of chloroform and added dropwise to

a stirring methanol (70 mL). Pure polymer formed as a precipitate and was collected by vacuum filtration before being dried in a vacuum oven at 70 °C overnight.

Table 10: Polymerisation reactions performed. Catalyst: monomer ratio was 1:800. All reactions carried out with a total of 16 mmol of monomer.

Entry	Molar Ratios		Monomer Mass (g)		Yield (g)	Yield (%)
	BL	LA	BL	LA		
P1	50	50	0.6887	0.9130	0.8520	53
P2	60	40	0.8265	0.7304	0.7962	51
P3	70	30	0.9642	0.5478	1.0705	71
P4	75	25	1.0331	0.4565	0.9168	62
P5	80	20	1.1020	0.3652	0.8932	61
P6	85	15	1.1708	0.2739	0.9123	63
P7	90	10	1.2397	0.1826	0.9036	64
P8	95	5	1.3086	0.0913	0.8626	62
P9	100	0	1.3774	0.0000	0.7294	53
P10	0	100	0.0000	1.8261	0.9403	51

5.2 POLYMER CHARACTERISATION

5.2.1 DSC

All DSC data was recorded on Mettler Toledo DSC 1 (Mettler-Toledo Ltd., Leicester, UK) with STARe acquisition and analysis software calibrated against an indium standard. The data was processed using STARe evaluations software. The DSC heating cycle was set to heat from -30-200 °C and the cooling cycle was set to cool the sample down to -30 °C. The heating/cooling rate was set at 10 °C/min This was done three times. The samples were weighed into 40 µl aluminium crucible with a lid clamped on.

5.2.2 TGA

All TGA data was recorded on Netzsch STA 449 simultaneous thermal analyser (NETZSCH-Gerätebau GmbH, Wolverhampton, UK). The raw data was opened in Microsoft Excel and subsequently processed using Origin2018b 64bit. The TGA programme was set to heat the sample from 25-450 °C with a heating rate of 5 °C/min, the 450 °C temperature was held for 2 minutes before cooling at a rate of 40 °C/min. The sample was weighed into an 25 µl aluminium crucible, with a lid clamped on

and a hole pierced in the lid. The sample was in an atmosphere of nitrogen with a flow rate of 20 mL/min.

5.2.3 GPC

GPC analysis was performed in chloroform on a Shimadzu Prominence GPC system (Shimadzu, Japan) equipped with a phenogel column. The polymer samples (20 mg) were dissolved in HPLC grade chloroform (6 mL), with care being taken to not agitate them. The solutions were filtered using polytetrafluoroethylene (PTFE) syringe filters from Fisher Scientific with 0.2 μm pores, into amber auto sampler vials from Fisher Scientific. The polymer samples were analysed with reference to polystyrene standards of known molecular weight.

5.3 FILM PREPARATION

5.3.1 Solvent Casting

This method was adapted from Wang *et al.*[78] The polymer sample (approximately 100 mg) was dissolved in chloroform (approximately 5 mL) by stirring for 5-6 hours. The solution was poured into a PTFE evaporating dish and left overnight to evaporate. The resultant films were peeled from the dishes and stored.

5.3.2 Spin Coating

The polymer sample was dissolved in chloroform by stirring for 5-6 hours. A spin coater machine (Spin Coater WS-650-23, Laurell Technologies Corporation, PA, US) equipped with a vacuum was used. A circular glass substrate (10 mm diameter) was saturated with the sample. It was then spun at 400 rpm for 3 minutes, 60 rpm for 30 seconds, 750 rpm for 90 seconds, then 190 rpm for 120 seconds.

5.4   FILM CHARACTERISATION AND TESTING

5.4.1 Testing for Suitability for Lining Single-Use Coffee Cups

5.4.1.1 Water Test

DI (75 mL) was heated to 95-100 °C and then poured (40 mL) onto a sample of polymer film. Once cooled, the film sample was removed and allowed to dry before storage. At the same time, room temperature DI water (40 mL) was poured onto another sample of the same film for the same amount of time. A sample of film was also kept as a control. The test where polymer film sample was submerged in DI water and 95 °C DI water were denoted as W2 and HW2 respectively.

5.4.1.2 Melt onto Paper

The film samples were prepared by solvent casting methods. Once fully dry, they were placed on top of uncoated cup paper, provided by the Printed Cup Company, and melted in an oven at 160 °C for 10-20 minutes.

5.4.1.3 Water Permeability Test using Cobalt Chloride Paper

To test water permeability, using a pipette, a sample of room temperature DI was placed on top of film coated paper, that had cobalt chloride paper underneath, for 10 minutes. The cobalt chloride paper was blue when it was anhydrous, however in the presence of water it changed colour to pink. How the cobalt chloride paper was made is described below.

$CoCl_2 \cdot 6H_2O$ (5 g, 38.5 mmol) was a purple solid. It was dissolved in water (100 mL) to form a red solution. Filter paper was soaked in the solution, which resulted in a colour change in the paper from white to pale pink. The filter paper was placed in an oven at 100 °C for 1-2 hours, until it had changed colour from pale pink to blue. The filter paper was sealed in a vacuum desiccator under argon to cool and be stored until use.[79]

5.4.1.4 Water Permeability Test using Fluorescein Dye

To test water permeability, a fluorescein dye solution was made at a concentration of 0.1 mg/mL in water. Using a pipette, approximately 1-2 mL was placed on top of the film coated paper and left for 24 hours.

5.4.1.5 Seam Test

The Printed Cup Company provided information on the manufacturing process of the cups. To form the cup shape, the card was folded around, and the PE was melted using ultrasonic heating and pressure along the overlapping seam to seal it. The same melting process was performed to add the base of the cup. This was tested with one of the polymer samples.

5.4.2 PXRD

Film samples were cut into a 1 cm by 1 cm piece and mounted in PXRD (Rigaku SmartLab, Tokyo, Japan). Counts were recorded against 2θ angle starting at 4 ° and finishing between 50-70 °. Data was processed using Origin 2018b 64bit.

5.4.3 SEM

Films were prepared for SEM by mounting them on a stub with adhesive carbon tabs, then coating them in gold using a rotary pumped cool (magnetron) sputter coater (Quorum Technologies Ltd Q150RES, Lewes, UK) . Images of the films were obtained using a SEM (Jeol JSM-7800F, Tokyo, Japan). EDX (X-Max50, large area 50 mm^2 Silicon Drift Detector (SDD) from Oxford Instruments, Abingdon, UK) was also used to evaluate what elements were present. Images were taken of the films before and after water exposure, so comparisons could be made.

6   BIBLIOGRAPHY

1   L. Galliers, Where will your coffee cup end up? Not in the recycling, https://conversation.which.co.uk/food-drink/recycling-disposable-coffee-cups-starbucks/, (accessed 28 November 2018).

2   House of Commons: Environmental Audit Committee, *HC 657 Disposable Packaging: Coffee Cups Second Report of Session 2017-19 Report, together with formal minutes relating to the report*, 2018.

3   PCRRG, PCRRG REPORTS HUGE INCREASE IN COFFEE CUP RECYLING, http://www.pcrrg.uk/case-studies/pcrrg-reports-huge-increase-in-coffee-cup-recyling, (accessed 11 September 2019).

4   Reality Check Team, Plastic recycling: Why are 99.75% of coffee cups not recycled?, https://www.bbc.co.uk/news/science-environment-43739043, (accessed 8 January 2019).

5   M. K. Marichelvam and M.Nagamathan, *Int. J. Eng. Technol. Sci. Res.*, 2017, **4**, 19–25.

6   R. Geyer, J. Jambeck and K. Law, *Sci. Adv.*, 2017, **3**, 25–29.

7   Costa, Our Cups, https://www.costa.co.uk/responsibility/our-cups/, (accessed 8 January 2019).

8   BBC, Coffee cup ban: Boston Tea Party's sales fall by £250k, https://www.bbc.co.uk/news/uk-england-bristol-47629820, (accessed 2 April 2019).

9   Paper Cup Recovery & Recycling Group, *PCRRG Progress Report*, 2018.

10   VTT Technical Ltd, Taking a closer look at paper cups for coffee, https://www.huhtamaki.com/globalassets/global/highlights/responsibility/taking-a-closer-look-at-paper-cups-for-coffee.pdf, (accessed 15 May 2019).

11   T. Webber, Paper Cups: A Responsible Consumer Choice, http://www.paperage.com/2019news/06_25_2019afpa_paper_cups.html.

12   M. Lackner, in *Kirk-Othmer Encyclopedia of Chemical Technology*, ed. K. Othmer, Wiley, Hoboken, New Jersey, United States, 6th edn., 2015, pp. 427–468.

13   BBC, Identifying plastics, http://news.bbc.co.uk/1/hi/magazine/7516859.stm, (accessed 8 January 2019).

14   Coda, Know Your plastic: Seven Plastics for Seven Recycling Possibilities, https://www.coda-plastics.co.uk/blog/know-your-plastic-seven-plastics-for-seven-recycling-possibilities, (accessed 8 January 2019).

15   V. Fombuena, D. García-Sanoguera, L. Sánchez-Nácher, R. Balart and T. Boronat, *J. Adhes. Sci. Technol.*, 2014, **28**, 97–113.

16   S. V. Meille, G. Allegra, P. H. Geil, J. He, M. Hess, J.-I. Jin, P. Kratochvíl, W. Mormann and R. Stepto, *Pure Appl. Chem.*, 2011, **83**, 1831–1871.

17   W. N. Dos Santos, J. A. De Sousa and R. Gregorio, *Polym. Test.*, 2013, **32**, 987–994.

18   James Cropper, James Cropper packages up example of circular economy best practice, https://www.cupcycling.co.uk/news/james-cropper-packages-up-example-of-circular-economy-best-practice, (accessed 8 January 2019).

19   J. K. Moon, S. U. N. Hyui Yoo and T. Shibamoto, *J. Agric. Food Chem.*, 2009, **57**, 5365–5369.

20   J. F. Carpentier, *Organometallics*, 2015, **34**, 4175–4189.

21   B. Pfister and S. C. Zeeman, *Cell. Mol. Life Sci.*, 2016, **73**, 2781–2807.

22   L. Xiao, B. Wang, G. Yang and M. Gauthier, in *Biomedical Science, Engineering and Technology*, ed. D. N. Ghista, IntechOpen, London, 1st edn., 2012, pp. 247–249.

23   A. K. Mohanty, M. Misra and G. Hinrichsen, *Macromol. Mater. Eng. 276*, 2000, **277**, 1–24.

24   R. O. MacRae, C. M. Pask, L. K. Burdsall, R. S. Blackburn, C. M. Rayner and P. C. McGowan, *Angewendte Chemie*, 2011, **50**, 291–294.

25   I. S. M. A. Tawakkal, M. J. Cran, J. Miltz and S. W. Bigger, *J. Food Sci.*, 2014, **79**, 1477–1490.

26   D. Garlotta, *J. Polym. Environ.*, 2002, **9**, 63–83.

27   S. Ebnesajjad, in *Polyvinyl Fluoride: Technology and Applications of PVF*, Elsevier Inc., Oxford, UK, 1st edn., 2013, pp. 251–263.

28   Y. Chen, L. M. Geever, J. A. Killion, J. G. Lyons, C. L. Higginbotham and D. M. Devine, *Polym. - Plast. Technol. Eng.*, 2016, **55**, 1057–1075.

29   A. Gupta, A. K. Pal, E. M. Woo and V. Katiyar, *Sci. Rep.*, 2018, **8**, 1–13.

30   T. Yamada, H. Tsuji and H. Daimon, *J. Environ. Manage.*, 2018, **226**, 476–483.

31   T. Häkkinen and S. Vares, *J. Clean. Prod.*, 2010, **18**, 1458–1463.

32   J. Lunt, *Polym. Degrad. Stab.*, 1998, **3910**, 145–152.

33   J. P. Lopez, J. Girones, J. A. Mendez, J. Puig and M. A. Pelach, *J. Polym. Environ.*, 2012, **20**, 96–103.

34   B. Lindley, Plastic recycling: just because it's plant-based (PLA plastic), is it better?, https://edgeenvironment.com/plastic-recycling-just-plant-based-pla-plastic-better/, (accessed 11 September 2019).

35   A. Soroudi and I. Jakubowicz, *Eur. Polym. J.*, 2013, **49**, 2839–2858.

36   M. P. Arrieta, M. D. Samper, M. Aldas and J. López, *Materials (Basel).*, 2017, **10**, 1–26.

37   C. A. Bishop, in *Vacuum Deposition onto Webs, Films and Foils*, Elsevier Inc., 3rd edn., 2011, pp. 85–128.

38   V. Taubner and R. Shishoo, *J. Appl. Polym. Sci.*, 2001, **79**, 2128–2135.

39   H. Brandl, R. A. Gross, R. W. Lenz and R. C. Fuller, *Adv. Biochem. Eng. Biotechnol.*, 1990, **41**, 77–93.

40   Y. Poirier, D. E. Dennis, K. Klomparens and C. Somerville, *Adv. Drug Deliv. Rev.*, 1992, **256**, 520–523.

41   M. Zinn, B. Witholt and T. Egli, *Adv. Drug Deliv. Rev.*, 2013, **53**, 790–794.

42   C. R. Hankermeyer and R. S. Tjeerdema, *Rev. Environ. Contam. Toxicol.*, 1999, **159**, 1–24.

43   J. Fagerland, A. Finne-Wistrand and D. Pappalardo, *New J. Chem.*, 2016, **40**, 7671–7679.

44   N. Altaee, G. A. El-Hiti, A. Fahdil, K. Sudesh and E. Yousif, *Springerplus*, 2016, **5**, 1–12.

45   H. Nishida, H. Ariffin, Y. Shirai and M. A. Hassan, in *Biopolymers*, ed. M. Elnashar, IntechOpen, London, 1st edn., 2010, pp. 369–386.

46   M. Erceg, T. Kovačić and I. Klarić, in *Polymer Degradation and Stability*, 2005, vol. 90, pp. 313–318.

47   M. P. Arrieta, J. López, A. Hernández and E. Rayón, *Eur. Polym. J.*, 2014, **50**, 255–270.

48   S. M. Lai, Y. H. Liu, C. T. Huang and T. M. Don, *J. Polym. Res.*, 2017, **24**, 1–12.

49   M. P. Arrieta, M. D. Samper, J. López and A. Jiménez, *J. Polym. Environ.*, 2014, **22**, 460–470.

50   N. Ljungberg and B. Wesslén, *Biomacromolecules*, 2005, **6**, 1789–1796.

51 L. Zhang, C. Xiong and X. Deng, *Polymer (Guildf).*, 1996, **37**, 235–241.

52 D. A. D'Amico, M. L. Iglesias Montes, L. B. Manfredi and V. P. Cyras, *Polym. Test.*, 2016, **49**, 22–28.

53 D. Puglia, E. Fortunati, D. A. D'Amico, L. B. Manfredi, V. P. Cyras and J. M. Kenny, *Polym. Degrad. Stab.*, 2014, **99**, 127–135.

54 A. Jordá-Vilaplana, V. Fombuena, D. García-García, M. D. Samper and L. Sánchez-Nácher, *Eur. Polym. J.*, 2014, **58**, 23–33.

55 D. Walton and P. Lorimer, *Polymers*, Oxford University Press, Oxford, 2000.

56 M. Bouyahyi, N. Ajellal, E. Kirillov, C. M. Thomas and J. F. Carpentier, *Chem. - A Eur. J.*, 2011, **17**, 1872–1883.

57 H. Abe, O. Doi, Y. Hori and T. Hagiwara, *Polymer (Guildf).*, 1998, **39**, 59–67.

58 B. J. Jeffery, E. L. Whitelaw, D. Garcia-Vivo, J. A. Stewart, M. F. Mahon, M. G. Davidson and M. D. Jones, *Chem. Commun.*, 2011, **47**, 12328–12330.

59 J. P. Macdonald, M. P. Parker, B. W. Greenland, D. Hermida-Merino, I. W. Hamley and M. P. Shaver, *Polym. Chem.*, 2015, **6**, 1445–1453.

60 E. D. Cross, L. E. N. Allan, A. Decken and M. P. Shaver, *J. Polym. Sci. Part A Polym. Chem.*, 2013, **51**, 1137–1146.

61 F. M. Kerton, A. C. Whitwood and C. E. Willans, *J. Chem. Soc. Dalt. Trans.*, 2004, **40**, 22372237–22442244.

62 X. Liu, X. Shang, T. Tang, N. Hu, F. Pei, D. Cui, X. Chen and X. Jing, *Organometallics*, 2007, **26**, 2747–2757.

63 E. L. Marshall, V. C. Gibson and H. S. Rzepa, *J. Am. Chem. Soc.*, 2005, **127**, 6048–6051.

64 M. Subramanian, *Polymer Testing*, Momentum Press, 1st edn., 2018.

65 Malvern Instruments, *Whitepaper*, 2015, **1**, 1–19.

66 B. L. Dutrow and C. M. Clark, X-ray Powder Diffraction (XRD), https://serc.carleton.edu/research_education/geochemsheets/t echniques/XRD.html, (accessed 3 July 2019).

67 M. C. Rowe and B. J. Brewer, *Comput. Geosci.*, 2018, **120**, 21–31.

68 IOWA State University, How the SEM Works, https://www.mse.iastate.edu/research/laboratories/sem/micro scopy/how-does-the-sem-work/high-school/how-the-sem-works/, (accessed 3 July 2019).

69   H. Andersson, J. Cramby, K. Sott, A. Bergstrand and A. Larsson, *J. Biomater. Nanobiotechnol.*, 2012, **03**, 431–439.

70   J. Shojaeiarani, D. S. Bajwa and N. M. Stark, *Carbohydr. Polym.*, 2018, **190**, 139–147.

71   M. A. Abdelwahab, A. Flynn, B.-S. Chiou, S. Imam, W. Orts and E. Chiellini, *Polym. Degrad. Stab.*, 2012, **97**, 1822–1828.

72   J. B. Zhu and E. Y. X. Chen, *Angew. Chemie - Int. Ed.*, 2019, **58**, 1178–1182.

73   M. Reiter, P. T. Altenbuchner, S. Kissling, E. Herdtweck and B. Rieger, *Eur. J. Inorg. Chem.*, 2015, **2015**, 1766–1774.

74   S. Ansari and T. Fatma, *PLoS One*, 2016, **11**, 1–20.

75   A. M. Harris and E. C. Lee, *J. Appl. Polym. Sci.*, 2007, **107**, 2246–2255.

76   K. W. Lin, C. H. Lan and Y. M. Sun, *Polym. Degrad. Stab.*, 2016, **134**, 30–40.

77   J. S. D'Arrigo, *Am. J. Physiol. Physiol.*, 1978, **235**, 109–117.

78   L. F. Wang, J. W. Rhim and S. I. Hong, *LWT - Food Sci. Technol.*, 2016, **68**, 454–461.

79   RSC, Preparing and using cobalt chloride indicator papers, http://www.rsc.org/learn-chemistry/resource/res00001919/preparing-and-using-cobalt-chloride-indicator-papers?cmpid=CMP00006709, (accessed 17 July 2019).